Akademie věd
České republiky

Thesis of Dissertation for Obtaining the 'Doctor of Sciences'
Degree in the Category of the Sciences
Chemistry

Chemistry and Physics of Surfaces and Biointerfaces: From Fundamental Understanding of Material Properties, Through Defined Biofunctional Interfaces, Towards Establishing Bio-autonomous Surfaces

Commission for the Doctoral Dissertation Defense in the Field of

Macromolecular Chemistry

Applicant's Name: ***Ing. Ognen Pop-Georgievski, Ph.D.***

Workplace of Applicant: **Institute of Macromolecular Chemistry, CAS**
Heyrovského nám. 2
162 00 Prague 6
Czech Republic

Place and Date: Prague, 12th November 2025

Summary of DSc. dissertation

The performance of devices used in different technical and industrial applications or involved in different chemical and physical processes depends on both the bulk properties of the materials they are made from, as well as on the structure and composition of their surface. The surface properties of a material can be affected to such an extent that the chemical nature of the underlying material becomes completely irrelevant (stealth effect). The presence of non-fouling densely end-tethered polymer chains (often termed as brushes) increases the bio-compatibility of implants or cell seeding scaffolds in various bio-medical applications. This allows for independent engineering of the structure, composition and design of the bulk material of particular device from its surface characteristics. In this manner the mechanical properties of the bulk can be completely or almost completely preserved. Additionally, the application of multi-functional polymer coatings allows decoration of a surface with distal end-groups capable of interaction with other molecules in their environment through specific molecular recognition processes. In attempts to mimic the autonomous behavior of living matter of biomaterial sciences and tissue engineering have recently focused on the design of biomimetic materials that are capable of eliciting specific cellular stimuli and directing new tissue formation mediated by biomolecular recognition, which can be manipulated by altering design parameters of the material. However, the true potential of these biomimetic concepts has not been entirely utilized and the physicochemical properties of performed polymer-based surfaces have not been fully understood.

The presented dissertation thus traces our efforts to develop and apply new concepts in synthesis of smart bioresponsive polymer surfaces, with defined physico-chemical properties and known state of incorporated bioactive groups. The emerging polymer chemistry, surface engineering and biofunctionalization concepts strive to outperform the contemporary polymer surfaces used as biomaterials, scaffolds and sensors, endeavoring the achievements towards autonomous self-regulating bioactive surfaces.

In the *Introduction* chapter, I will critically delimit currently accepted macromolecular avenues for the synthesis of biofunctional interfaces, stating the advantages and disadvantages of adopted principles and applications.

In the first part of the thesis, I will focus on our achievements in *the creation of self-assembled monolayers of chlorosilanes, bisphosphonates and biomimetic polydopamine (PDA) films for the modification of various classes of materials and surfaces*. Mainly I will report on our contribution in understanding the growth rate, morphology and covalent structure of *surface adherent films based on PDA*. This bioinspired polymer, also known as synthetic melanin, is widely used as an anchoring layer for the modification of various solid substrates, even though its chemical structure is rather elusive. Even more, it is not evident to which extent the chemical nature of the substrate, on which the layer is formed, influences and predetermines the covalent structure of resulting surface adherent PDA films. We have studied the growth of PDA using a plethora of surface-sensitive techniques which have been adopted and further developed in our department, such as spectroscopic ellipsometry, atomic force microscopy and X-ray photoelectron spectroscopy. We utilized grazing angle attenuated total reflection Fourier-transform infrared spectroscopy (FTIR) with multivariate statistical analysis to further gain analytical power and probe the covalent structure of the surface confluent films on the macroscopic scale. Furthermore, we probed the structure on the nanoscale by utilizing scattering-type scanning near-field optical microscopy (sSNOM) and nanoFTIR spectroscopy. It was found that the polymerization process leads to a formation of a surface confluent PDA layer and deposition of PDA nanoaggregates. We found notable differences in the chemical composition of PDA surface confluent films depending on the polymerization time and type of substrate used. The differences in the optical contrast observed at irradiation energies corresponding to the vibrations of indole units of PDA and quinoid groups of polymerization intermediates indicated a different composition of the nanoaggregates and the surrounding confluent layer. At the later stages of layer formation, a unified structure was observed over the surface independently on type of solid substrate.

In the second part of the thesis, I will address *the macromolecular and biofunctionalization approaches that we have developed for the purpose of controlling adverse adsorption effects on artificial surfaces contacting biological media*. The presence of hydrophilic densely end-tethered polymer chains can circumvent the detrimental non-specific adsorption of proteins on artificial surfaces thus surpassing the bio-compatibility issues of implants, increasing the specific response in biosensors towards the specific detection of analytes or guiding specific interactions of cell seeding scaffolds. These densely packed polymer chains can be obtained via two main approaches consisting of grafting of performed polymer chains to a surface (termed as “grafting-to” approach) or by growing the polymer chains from active centers present on the material surface (termed as “grafting-from” approach) via various controlled radical polymerization methods. I will summarize our achievements in synthesizing different polymer brushes via the two methods, ranging from polyethylene oxide-, polyoxazoline-, polyoxazine-, poly(meth)acrylate- and poly(meth)acrylamide-based brushes. A particular emphasis is set on *physical-chemistry of polymers and surfaces*, through the precise determination of: the covalent structure and surface related parameters of adherent polymer chains; solvation and effect of various salts in the Hoffmeister series; z-profile of the chemical composition of the polymer surfaces and brushes; organization of water molecules present in the hydration shell of the polymer brushes; the content, surface density and accessibility of distal-ends. Utilizing infrared nanoscopy based on sSNOM and nanoFTIR, we unravel not only the chemical composition of polymer layers on the nanoscale, but also reveal the orientation of chains constituting the polymer brushes. Finally, within this section we will contrast the non-fouling properties of polymer brushes of various chemical structure. Furthermore, on the example of poly[*N*-(2-hydroxypropyl)methacrylamide], we will provide an accurate comparison between brushes created via grafting-to and grafting-from approach of same molecular properties in terms of the ability to resist fouling. A crucial part of this section was developing the single molecule force spectroscopy analysis protocols for the analysis of polymer brushes synthesized via the grafting-from approach.

In the third part, I will address the application of *developed bioactive polymer-based systems as functional interfaces for biosensing and biomedical applications*. This will be achieved through reporting our works on specific detection of protein biomarkers in biological media and the design of implantable materials based on anti-fouling hierarchical brushes bearing extracellular matrix-derived peptide motifs.

In the final chapter, I will focus on the direction stemming from this thesis, our visions beyond the paradigm of eternal canceling of fouling when tissue engineering applications are in question and the challenges we need to face ahead. Inspired by nature and the ability of cells not only to react when exposed to external stimuli but also to remodel the material and environment which they contact we propose autonomous surfaces. These will deliver the necessary signals to adherent cells but also will guide their own fate while in close relation to the cell behavior. This would imply that the envisioned surfaces would not be only biomimetic and biodegradable, but will have encoded autonomous responses depending on the communication and behavior of surface adherent cells. Any progress in this direction might be beneficial in the next generation of not only advanced biomaterials and medical devices such as stimulators, sensors, stents, etc., but also environmental sensors, self-regulating appliances and other domains demanding autonomy.

Table of Contents

Introduction

The uniqueness of living matter. The living matter/organism shows particular unique characteristics like autonomous adaptation, growth, metabolism, reproduction, self-organization, self-replication, interaction with the surrounding, the ability to sense and react to these external stimuli.[1] Living organisms have the ability to undergo various changes as a result of different external impulses, but also can efficiently reconstruct the surrounding depending on the needs of their life cycle.[2] These characteristics clearly set apart the living from the non-living matter, which lacks these integral biochemical-responding mechanisms.

Current paradigm of everlasting bioactive intelligent surfaces. In attempts to mimic the autonomous behavior of living matter of biomaterial sciences and tissue engineering have recently focused on the design of biomimetic materials that are capable of eliciting specific cellular stimuli and directing new tissue formation mediated by biomolecular recognition, which can be manipulated by altering design parameters of the material.[3] The performance of devices used in different technical and industrial applications or involved in different chemical and physical processes depends on both, the bulk properties of the materials they are made from, as well as on the structure and composition of their surface.[4] In order to control the interaction of a material with its environment, coatings of thin and even monolayer polymer films are frequently applied to the surface of these solids.[5] The thin coating, composed of polymer chains densely end-tethered (often termed as polymer brushes) to the surface of materials can significantly improve the properties of objects as they allow controlling the interaction of the material with its environment.[6, 7]

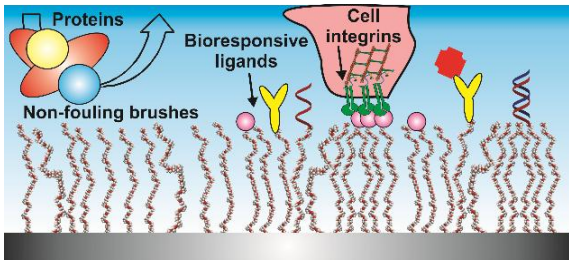

Fig. 1. *Bioresponsive ligands (integrin binding peptides, antibodies, DNA strands) immobilized at the distal-ends of non-fouling polymer brushes. The polymer background suppresses the non-specific interactions and elicits the built-in "information" molecules to the environment.*

In biomedical and bio-technological applications and devices, a monolayer coating of hydrophylic polymer brushes allow for control of the interaction between biological environment, e.g., cells and bio-molecules, and the artificial materials (***Fig. 1***). Hydrophobic methacrylate-based fluoropolymer brushes have been pursued as an alternative path for the creation of non-fouling layers capable of suppressing the fouling from blood to 7±5 ng/cm^2.[8] Even more desired but rarely achieved, 100% prevention of the nonspecific adsorption of proteins onto the surface, was recently reported by the PI's research team submitting this project.[9-12] The presence of such a truly non-fouling brushes based on polyethylene oxide, poly(carboxybetaine acrylamide) (PCBAA), poly(carboxybetaine methacrylamide) (PCBMA) and poly(*N*-(2-hydroxypropyl) methacrylamide) (PHPMA) increases the bio-compatibility of an implant or cell seeding scaffold.[13-19] Similarly, efficient label free sensing of important analytes, e.g. pathogens that are present in different media, can be performed only in presence of a protein repulsive polymer background.[20-23] Spatially ordered/arranged regions of such non-fouling polymer backgrounds are crucial for lab-on-a-chip and micro-array applications. Particular polymer coatings affect the surface properties to such an extent that the chemical nature of the underlying material becomes completely irrelevant (stealth effect). This allows for an independent engineering of the structure, composition and design of the bulk material of particular device from its surface characteristics.[4, 6] In this manner the mechanical properties of the bulk can be completely or almost completely preserved.[5-7] Additionally, the application of multi-functional polymer coatings allows decoration of a surface with distal end-groups capable of interaction with other molecules in their environment through specific molecular recognition processes. Such a modification strategy gains exceptional importance, for example, for control of the adhesion of living cells to artificial substrates.[24] In such a case, thin polymer layers enriched with cell recognition peptide sequences derived from extracellular matrix proteins can induce strong specific adhesion and proliferation of the cells on the artificial substrate surfaces.[24-33] As a rule of a thumb it has been accepted that the inert polymer background elicits the specific information incorporated at polymer chain distal-ends, i.e. terminal group of the polymer chain. Indeed, the translation of the developed concepts to tissue engineering and the creation of biodegradable scaffolds lead to

functional *de novo* tissues.[30, 34-38] The bioengineering concepts based of de-cellularized tissue which has been reseeded with has shown that the cell/material interface plays a crucial role in guiding and determining the cells fate and can drive the behavior of living matter at interfaces.[38-41] The current paradigm of controlling the complex interactions on the device surface/cells interface is founded on the synthesis of such everlasting non-fouling polymer brush surfaces carrying cell-instructing signaling cues inspired from the proteins constituting the extracellular matrix (ECM).[13, 19, 42-48] Thus, the concomitant canceling of the non-specific interactions and the delivery of specific information to the cells has been expected to lead to normal behavior of the cells and acceptance of the implanted device by the host organism. However, the currently accepted concepts for the surface modification of biomedical devices underestimate the cell-material interactions in the phase of the extra-cellular matrix formation (***Fig. 2***). While the detachment of the adherent cell-matrices from the bioactive polymer brush can be utilized as a concept for selective cell harvesting, the concept seems to be destined to failure when implants are being in question. This implies that any of the current efforts utilizing the established paradigm are destined to failure and calls in for immediate action.

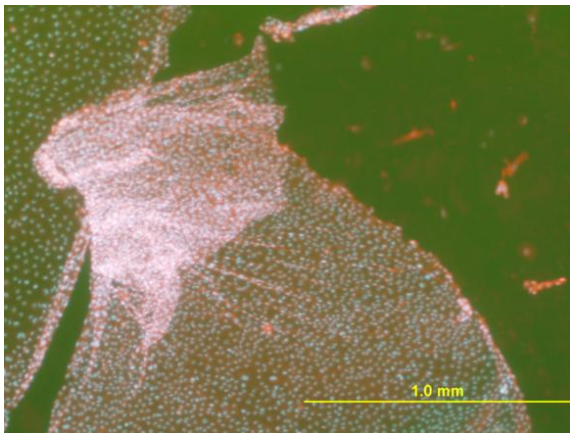

Fig. 2. *Detachment of bovine pulmonary artery endothelial cells on non-fouling polymer decorated with 700 fmol/cm² RGD bioactive sequences after 7 days of cultivation.*

A nature inspired challenge: Bio-active interfaces that undergo autonomous adaptation. Nature answers this problem through the autonomous adapting ability of living organisms and their environment. [1-3, 49-51] This duality does not infer only to the cells ability to respond, adapt and reconstruct their environment, but goes beyond and depends on the inherent encoding of the cells environment/ support to undergo similar autonomous processes. Bio-mimicking and -inspiration concepts are being widely studied and explored. The development and the investigation of artificial macromolecular biomimetic and bio-analogous systems is a long-standing challenge. However, the fields of surface and material science are far from achieving the stated duality concept and mainly concern particular material-based responses of non-living matter. While self-healing, pH, pI and temperature responses of non-living matter [52-55] have been well described in respect to the physicochemical nature of underlying phenomena, we can state that these processes only mimic particular aspects of living matter, and do not represent living matter's collective autonomous behavior. The construction of materials and surfaces with this autonomous responsiveness that mimics living systems remains still an unsolved scientific problem.

In a long term, the team's objective is to change the current paradigm when surface modification of implantable devices is in question. This clearly means, developing novel concepts for the preparation of synthetic smart bio-responsive polymer surfaces, with defined physicochemical properties and known state of its bioactive distal end-groups. At the same time the smart surfaces should have unique property of selective guidance of their own fate which bring them closer to the behavior of living matter. This is envisioned to be achieved through encoding responses/events in direct relation to the behavior, responses and communication of the surface adherent cells, which will set the layers as bio-analogous and bio-autonomous.

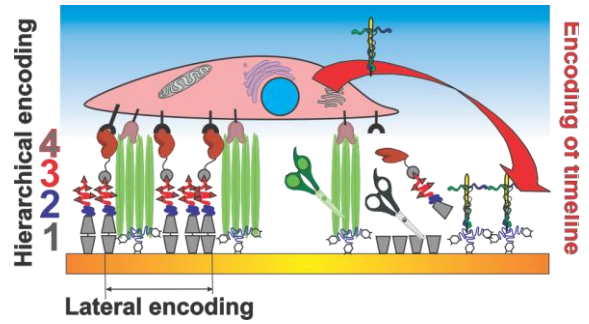

Fig. 3. *Envisioned surface with lateral, hierarchical and time-line encoding which autonomously responds to the surrounding allowing the restructuring of the surface.*

This is a hard goal with several inherent challenges connected with the development of

macromolecular chemistry avenues and biofunctionalization for bio-autonomous encoding and precise characterization of these not only on the macroscale but also on the nanoscale (***Fig. 3***).The advent of controlled polymerizations (CP) and click chemistry reactions lead to the possibility of precise tuning of the macromolecular architecture.[56-64] To cope with new challenges and requirements posed by the need for highly specialized materials, in particular the need of having molecular structures which have depth and lateral hierarchy, further advances in the control of architecture are imperative. New biomedically relevant polymers should be developed to avoid the newly reported compromised PEO based platforms which have been radially recognized by human's immune system. Newly developed (meth)acrylate, (meth)acrylamide, 2-alkyl-oxazoline and 2-alkyl-oxazine monomers bearing alkyne, azide- and fluorinated side chains enabling antifouling properties and at the same time the [15, 23, 65-67] fine tuning of surface adherent architecture of homo and/or multiblock polymers. The selection of other monomers and control of polymerization can be utilized for the achievement of hierarchical structuring on the vertical scale of the polymer layers. Lateral control of the layer structuring can be achieved by adopting be achieved by merging new types of CPs and photo-induced modular/orthogonal conjugation reactions. Specifically, through the synthesis of "traditional" and bioinspired anchor layers (dopamine–, catechol–based layer-by-layer (LbL) structures or other biopolymers such as polysaccharides, tannic acid or curcumine–based LbL) that would provide strong anchoring points for the creation of the polymer architectures, but also a subsequent strong anchor of the *de novo* synthesized ECM which will replace the architecture.Though the synthesis of peptide-based initiator moieties that would provide surface initiation of CP and at the same time would provide the possibility of the surface adherent polymer to be cleaved by extracellularly expressed proteases or by pH lability, one can envisage the encoding of a timeline of events through the surface will autonomously respond to the surrounding and allow the reconstruction. Of particular interest remains on optimization of the solution and surface-initiated (SI) CPs atom transfer radical polymerization (SI-ATRP), photoinduced single electron transfer-living radical polymerization (photo-SET-LRP) and surface-initiated reversible addition fragmentation chain transfer radical polymerization (SI-RAFT) and lining cationic ring opening polymerization (CROP) with emphasis set on end-group-fidelity (necessary for conjugation and encoding) as well as in the molecular mass distribution of the polymers synthesized in solution and from the surfaces. The lateral structuring and encoding can be achieved through photo-induced Diels-Alder "click chemistry" reactions for the creation of different polymer architectures and different lithographic methods (photo-lithography, simple colloidal lithography, direct laser ablation, nano-contact printing etc.) to develop lateral patterns for the synthesis of proteolysis-cleavage induction points, biofunctionalization of the surfaces with a library of ECM derived-, hormone mimicking-, cadherin derived- peptides.

Understandably, the envisioned autonomous encoding of the surfaces demands detailed analytical characterization and understanding the physico-chemical properties the prepared surfaces. The primarily focus is set on the covalent and conformational state of the end-tethered polymer chains, the precise determination of surface concentration, distribution and availability of the different distal end-groups (neutral, reactive and bioactive) on the polymer brushes, for example bioadhesive motifs, as well as on their availability for further interactions and determination of the time encoding. Thus, a complete understanding of the physico-chemical surface properties can be achieved through:

a) determination of the composition and covalent structure, thickness, grafting density, wettability and surface free energy of the synthesized polymer layers;
b) spectral calculations enabling better understanding of the observed spectral features obtained by different spectroscopies;
c) addressing the solution properties of the newly synthesized polymers such as solvation, rigidity of the coil, existence of assemblies;
d) determination of the z-profile/hierarchical arrangement of the chemical composition of the layers of different architectures, their conformation, flexibility, morphology and interaction with water;
e) identification, determination, optimization and characterization of the encoded biodegradability;
f) visualization, mapping and probing of the strength between the bioactive surface immobilized molecules and its counterparts by fluorescence microscopy, and advanced atomic force microscopy (AFM) measurements such as single-molecule force spectroscopy (SMFS);

g) characterization of the surfaces at scale below the diffraction limitations of “traditional” spectroscopies.

At the protein level of cells adherent to ECM or artificial surfaces, the components of the focal adhesion plaques, gap junctions and differentiation molecules are traditionally, investigated by immunofluorescence staining followed by conventional and special microscopic techniques. The conventional techniques include standard epifluorescence microscopy and confocal laser scanning microscopy. The super-resolution microscopy methods acquire confocal images (optical sections) with axial resolution beyond the conventional limits. The optical sections are about 300 nm in thickness, which is about 3 times better than in confocal laser scanning or spinning disk microscopes. Optimizations of methods allow the recording of super-resolution images, which preserve details of about 125 nm in the lateral dimension, double the conventional resolution of optical microscopes enabling studying the fine 3D structure of cells. *Single molecule localization microscopy* is another super-resolution technique based on the photo-activated localization microscopy/stochastic optical reconstruction microscopy.[68-70] However, all these great advances in microscopy concern biology and mainly focus on the protein level or studying the cell responses with relation to the underneath material. Obviously, none of these super resolution techniques provide sufficient spectroscopic chemical information of the polymer films, and conclusions need to be “indirectly” derived.

High lateral resolution supplemented with spectroscopic information can be obtained utilizing near-field spectroscopies.[71-73] NanoFTIR is based on scattering-type scanning near-field optical microscopy (*s*SNOM) where infrared images with nanoscale spatial resolution are obtained by recording the infrared light scattered at a scanning probe tip. The probe is typically a metalized AFM tip. Acting as an antenna, it concentrates the incident field at the tip apex for local probing of molecular vibrations, similar to tip-enhanced Raman spectroscopy. When the AFM tip is illuminated by the broadband infrared radiation, Fourier transform spectroscopy of the scattered light yields infrared spectra with a spatial resolution down to 20 nm.[74-78] Two near-field FTIR operational modes have been demonstrated one with interferometric design and optical detection methodology for the detection of scattered light [73, 79-81] and the other based on detection of photothermal expansion, often termed as nanoFTIR and AFM-IR, respectively.[82] NanoFTIR has been used for studying biological objects such as protein fibrils and probe their secondary structure, membranes, viruses, polymer blends, nanocellulose material etc.[76-78, 80, 83-85] Recently, my team has successfully used to determine the orientation of ultrathin PEO polymer brushes at levels close to tents of chains.[86] The technique does not only give the chance of giving spectroscopic information on the nanoscale through lateral chemical mapping, but also has been demonstrated that can bring valuable information on the hierarchical structuring along the surface normal.[85] While very powerful to for studying various types of surfaces, near-field FTIR spectroscopies have been rarely used to probe *in situ* the interface between surfaces and cells.[87] Understandably, this is a very hard task stemming from the inherent problems of strong interference of IR radiation with water and presence of cells which will oversaturate the IR spectra with signals.

Chapter 1 – Self-assembly of anchoring layers [D1-D5]

The ability to functionalize material surfaces with high precision and reproducibility is central to numerous technological and biomedical applications, including biosensors, medical implants, microfluidic devices, antifouling coatings, and cell-instructive scaffolds. The properties of a surface, such as its chemical functionality, wettability, roughness, and biocompatibility, critically influence how it interacts with its environment, particularly in complex biological fluids. Among the most widely used strategies for surface modification of precious metal, metal oxide and in general oxide surfaces are the formation of self-assembled monolayers (SAMs) using thiol-, alkoxysilane-, chlorosilane-,

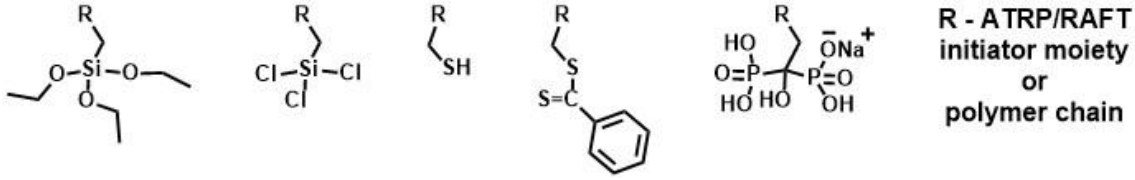

Fig. 4. *Various moieties employed for anchoring of self-assembled monolayers and polymers.*

phosphonate- and bisphosphonate-terminated organic molecules (***Fig. 4***). These low-molecular-weight modifiers offer strong, covalent anchoring to precious metal and hydroxylated surfaces such as glass, silicon oxide, titanium dioxide, and other metal oxides, while presenting functional end-groups for further chemical reactions.

Thiol-terminated self-assembled monolayers (SAMs) are widely used as initiator platforms for SI-CRP, enabling the fabrication of polymer brushes with precise control over thickness, composition, and architecture. These SAMs are typically formed through the chemisorption of thiol-functionalized initiator molecules onto gold (and other noble metal substrates such as copper, silver, platinum, etc.), taking advantage of the strong Au–S interaction to create robust, well-ordered monolayers.

Chlorosilanes, such as alkyl- or aryl-substituted trichlorosilanes, react with surface hydroxyl groups through a condensation reaction, forming robust Si–O–metal bonds. The resulting monolayers are relatively stable and allow for tuning of surface energy, charge, and chemical reactivity. For example, monofunctional chlorosilanes terminated with alkyl, amino, carboxyl, or polyethylene oxide (PEO, also termed as polyethylene glycol (PEG)) groups can be used to tailor wettability or enable biomolecule attachment. However, care must be taken during their deposition, as in the case of alkoxysilanes, to avoid multilayer formation or hydrolytic degradation.

Common ATRP initiator groups incorporated into both of thiol- and chlorosilane-terminated SAMs include alkyl halides such as 2-bromoisobutyrate and 2-chloropropionate, both of which effectively mediate controlled radical polymerization. These halide-functionalized SAMs present high densities of initiation sites, supporting uniform and dense polymer brush growth. The ability to finely tune polymerization conditions using these initiators has enabled the development of advanced surface coatings with tailored properties. The use of SAMs in SI-ATRP and SI-RAFT supports diverse applications in biosensing, antifouling coatings, micro- and nanopatterning, and stimuli-responsive surfaces. On the basis of XPS analysis we have developed a method for calculating the surface density of initiating and CTA moieties present in the SAM.[88, 89] The initiator SAM's provide Br- and Cl-based initiator densities of ~4–5 halogen atoms/nm². These significantly exceed the final brush densities of ~0.5–0.7 chains/nm², achievable through SI-ATRP and photoinduced SET-LRP indicating efficient initiation without surface saturation.[88] At the same time, the exchange of the Br atom for a chain-transfer moiety resulted in 2–3 CTA groups /nm². [89, 90] The XPS analysis approach could be directly applied for the determination of the surface density of peptide ligands present on polymer brush surfaces.[91] Additionally, the monolayers can be further functionalized or patterned prior to polymerization, expanding their versatility in surface engineering. Although challenges remain in achieving perfectly uniform initiator coverage, SAMs bearing initiator moieties to play a critical role in precision surface modification via SI-ATRP and SI-RAFT.

Bisphosphonates, originally developed for osteoporosis treatment, have also emerged as effective surface modifiers due to their high affinity for metal ions. Molecules such as neridronate form stable mono- or bidentate complexes with surface titanium or zirconium atoms.[92] Upon binding, the bisphosphonate forms a chemically resistant and well-organized monolayer, which can serve as a primer for further modification. This approach is particularly relevant for titanium-based biomedical devices where direct anchoring of functional polymers or bioactive ligands is required. While chlorosilanes and bisphosphonates enable efficient surface functionalization, their use is largely limited to substrates with specific oxide chemistries and requires stringent control over moisture and deposition conditions.

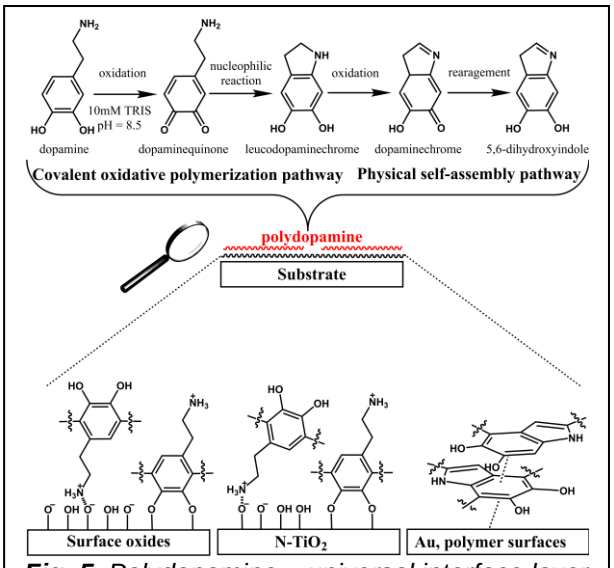

Fig. 5. *Polydopamine – universal interface layer that provides a "substrate—independent" anchoring.*

To overcome these limitations and to offer greater substrate versatility, biomimetic surface coatings based on polydopamine (PDA) have gained importance (***Fig. 5***). Inspired by the adhesive proteins of marine mussels, PDA can be

deposited from dopamine in mildly alkaline aqueous solutions (pH ~8.5). PDA forms stable coatings on virtually any material, including metals, oxides, ceramics, polymers, and even superhydrophobic surfaces. PDA coatings are formed via the spontaneous oxidative polymerization of dopamine in the presence of dissolved oxygen. The resultant thin film is rich in functional groups such as catechols, quinones, amines, and imines, which provide multiple points of reactivity. These groups allow for the subsequent grafting of polymers, peptides, or other ligands via Michael addition, Schiff base formation, or metal coordination. Unlike thiols, silanes and (bis)phosphonates, PDA coatings do not rely on specific surface chemistries and are not restricted to oxide-bearing substrates. This universal adhesion has positioned PDA as a uniquely versatile platform for surface functionalization in both material science and bioengineering. The combination of PDA's simplicity of application, its broad substrate compatibility, and its reactive surface chemistry makes it an attractive choice for a wide range of applications. However, despite its widespread use, many aspects of PDA formation remain insufficiently understood. In particular, the influence of substrate chemistry on PDA growth kinetics and structure, the dual presence of surface-adherent films and nanoaggregates, and the chemical uniformity of the resulting coatings.

We presented a comparative study of PDA film formation on various planar surfaces. Building on our previous efforts to optimize surface coatings via thiols, chlorosilanes and bisphosphonates, we now direct our attention to understanding the mechanisms and properties of biomimetic PDA layers as a multifunctional surface platform. By analyzing PDA formation across substrates and deposition times using a variety of surface-sensitive and nano-spectroscopic tools, we aimed to delineate the parameters that control its morphology, chemical composition, and structural homogeneity. The insights gained from the works focusing on bioinspired anchoring layers are expected to result in a more rational design of PDA-based coatings for the achievement of autonomous bioactive surfaces. Understanding the structural complexity and chemical composition of PDA films requires a multifaceted analytical approach. Given the dual morphology of PDA, comprising of a surface-confluent layer and discrete surface attached nanoaggregates, conventional bulk methods are insufficient to resolve the chemical heterogeneity and nanoscale organization of these coatings. Therefore, a group of complementary techniques has been used to characterize PDA films across multiple scales, from the macroscopic to the nanometric scale.

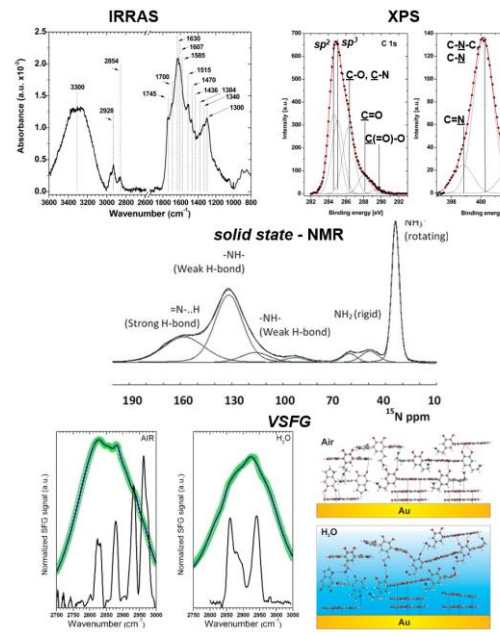

Fig. 6. *Various far-field spectroscopies point to PDA's complex structure and presence of ethylamine moieties that did not underwent the cyclization process. Solid state NMR and VSFG point to presence of organized structures in which the non-cycled structures are "sandwiched" between aromatic rings.*

1.1 Polydopamine covalent structure, growth kinetics and morphology. [*D5-D16*]

The formation of PDA films begins with the oxidative polymerization of dopamine in an alkaline, oxygen-rich aqueous environment. The reaction leads to the generation of a complex mixture of intermediates including dopamine-quinone, 5,6-dihydroxyindole, and other redox-active intermediates. These species undergo further reactions to form insoluble oligomers and eventually adhere to the surface either through direct adsorption or surface-initiated polymerization.

The IRRAS spectra of 20 nm thick PDA surface confluent films have a broad character with poorly resolved bands. In line with our XPS [93], solid-state NMR [94-96] and vibrational sum-frequency generation spectroscopy (VSFG) studies on PDA, our IRRAS spectra of PDA films on gold substrates show CH stretching bands at 2857 and 2930 cm^{-1} (***Fig. 6***).[17] These bands are characteristic of CH_2 asymmetric and symmetric stretching modes arising from the ethylamine aliphatic chains of dopamine and dopamine quinone monomer units that did not undergo spontaneous oxidation and

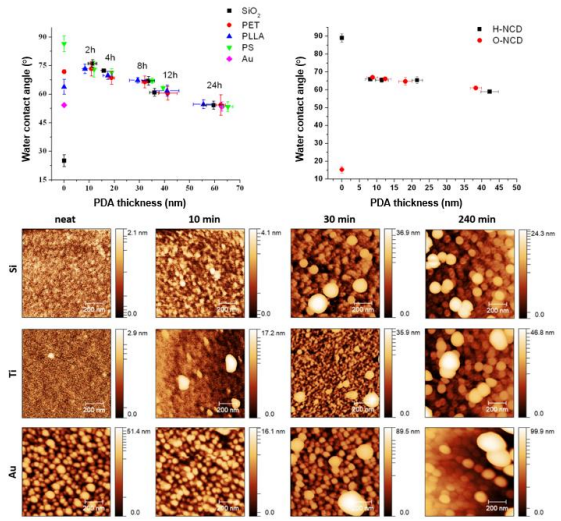

Fig. 7. *Evolution of water contact angle with growing thickness of surface confluent PDA layer on substrates with different surface energy. The growth of PDA leads to pronounced surface morphologies of increasing roughness due to the presence of nanoaggregates.*

intramolecular cyclization during the polymerization/deposition process. In the fingerprint and amide I regions (1000–1800 cm^{-1}) the spectrum of neat surface adherent PDA films show many overlapping vibrational modes. The strong bands at 1700 and 1745 cm^{-1} can be assigned to the C=O stretching vibration of hydrogen-bonded and free (non-hydrogen-bonded) quinone groups, respectively. The bands at 1436, 1585, 1607, and 1628 cm^{-1} arise from the C=C aromatic ring vibrations of the different PDA subunits.[97, 98] Some of these bands have small contributions from the NH_2 scissoring mode. The presence of pyrrole rings in PDA can be confirmed by the presence of bands at 1384 and 1473 cm^{-1}. The amino group also gives rise to bending mode bands at 1515 cm^{-1} and C–N stretching modes at 1340 cm^{-1} which are coupled to the indole ring vibrations. The O–H deformation and C–O stretching mode can be seen at 1210 and 1300 cm^{-1} respectively. All observed spectral features confirm the complex structure of the PDA films.[11, 17]

A typical PDA film growth curve exhibits two main phases: an initial rapid linear growth followed by a plateau phase. This biphasic behavior has been confirmed by spectroscopic ellipsometry (SE) studies conducted on various substrates including silicon dioxide, gold, titanium oxide, nanocrystalline diamond substrates of oxygen and hydrogen termination, polystyrene and polyethylene terephthalate substrates. In the first 30–60 minutes, SE measurements revealed a steep increase in film thickness, reaching values between 10–20 nm, depending on the substrate (***Fig. 7***). After this period, the growth rate slows down significantly, often plateauing around 20–30 nm, likely due to dopamine depletion or oxygen limitation in the reaction medium.[12, 93, 99-101] The transition from a thin surface-seeded layer to a fully confluent polymeric film is accompanied by morphological changes. AFM measurements show that within the first 10 minutes of polymerization, only sparse clusters or low-density aggregates are present on the surface. These features are generally less than 10 nm in height and widely spaced. As deposition proceeds, these islands grow and coalesce into a continuous film by the 30-minute mark. [100] The surface roughness of PDA films increases during the early growth phase but then stabilizes as the layer becomes confluent. For example, PDA layers formed on nanocrystalline diamond (NCD) substrates showed a steady increase in root-mean-square (RMS) roughness from 10 nm at 2 hours to 30 nm at 24 hours, along with a corresponding increase in grain diameter and height.[93] Importantly, these morphological transitions are not merely topographical; they also reflect underlying changes in chemical composition and organization, which are discussed in later sections. One notable aspect of PDA deposition is its simultaneous formation of both a surface-adherent continuous layer and suspended nanoaggregates in solution. These aggregates, which can be up to 100 nm in size, often settle onto the surface during or after the formation of the primary film, creating a complex, hierarchical morphology. A reasonable question has risen and that to which extent of the surface confluent films and nanoaggregares of PDA are of identical chemical structure. sSNOM and nanoFTIR studies have revealed that these nanoaggregates are not chemically identical to the underlying film, often containing higher concentrations of certain functional groups such as quinones or indole units. [99, 100]

Despite the complex nature of the deposition process, PDA films exhibit remarkable reproducibility in terms of thickness and topography when reaction conditions are carefully controlled. However, the early-stage variability, particularly in the formation and distribution of nanoaggregates, suggests that substrate chemistry, surface energy, and roughness play non-negligible roles in shaping the ultimate film architecture. The dual-mode film formation, surface-

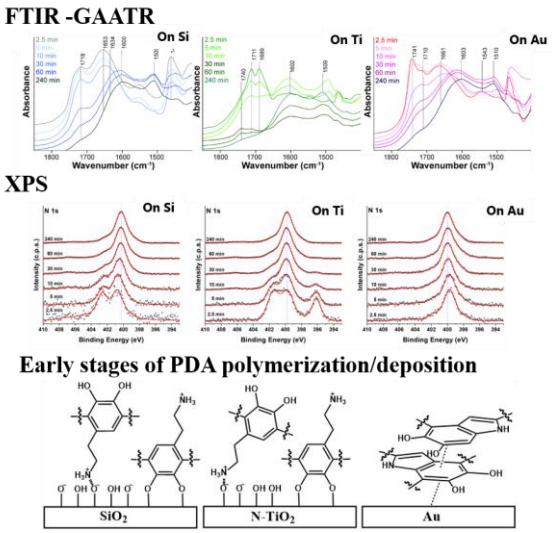

Fig. 8. *Evolution of GAATR-FTIR and high-resolution XPS spectra taken in the N 1s region for surface confluent PDA layer after different deposition/polymerization times. In the early stage the PDA chemical composition is strongly influenced by the substrate properties.*

mediated polymerization and aggregate deposition, provides both opportunities and challenges for applications. On the one hand, nanoaggregates may increase surface area and reactivity, beneficial for catalysis or biosensing. On the other hand, uncontrolled aggregation may impair film uniformity, limit transparency, or introduce chemical heterogeneity, making rigorous control of deposition parameters essential. In the following section, we delve deeper into how different substrate materials influence the PDA deposition process, focusing on how variations in surface chemistry, oxide termination, and topography affect the growth kinetics and covalent structure of PDA films.

1.2 Substrate influence on PDA film properties. [*D10, D13, D15-D17*]

Although polydopamine is often described as a "substrate-independent" coating due to its ability to adhere to nearly all material types, our recent studies reveal that the nature of the underlying substrate exerts a significant influence on the early stages of PDA formation (***Fig. 8***). This effect manifests in differences in growth kinetics, surface roughness, aggregate formation, and even chemical structure—particularly within the first hour of deposition. Experiments comparing PDA deposition on substrates such as gold (Au), silicon/silicon dioxide (Si/SiO_2), nitrogen doped titanium oxide ($N\text{-}TiO_x$), and NCD have revealed systematic variations in the film's thickness and morphology over time. On Au surfaces, the initial rate of PDA deposition is notably higher, with early-stage thickness values exceeding those observed on oxide surfaces for equivalent deposition times.[12, 93, 99, 100] This is attributed to favorable π–π stacking interactions between the aromatic units of dopamine and the hydrophobic Au surface, which lacks hydroxyl groups but supports van der Waals and electronic interactions. In contrast, on hydroxylated oxide surfaces like Si/SiO_2 and $N\text{-}TiO_x$, hydrogen bonding and coordination interactions dominate the initial binding. These interactions promote more controlled, layer-by-layer growth but may initially retard the polymerization rate. Indeed, far-field GAATR-FTIR and XPS analysis (***Fig. 8***) showed that PDA films on oxide substrates initially contained a higher proportion of uncyclized dopamine and catechol units, whereas PDA on Au featured more quinonoid and indole-like structures within the same time frame.[99-101] This substrate dependence is also reflected in the adhesion and distribution of PDA nanoaggregates. On hydrophilic oxide substrates, aggregates tend to be smaller and more evenly dispersed, likely due to better wetting and fewer hydrophobic interactions.

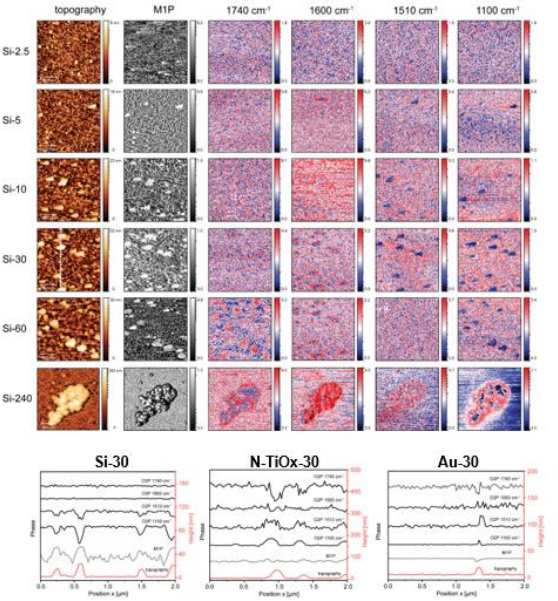

Fig. 9. *IR* sSNOM *images of PDA layers on the Si/SiO2 surfaces. The samples were studied at 6 different times of PDA deposition (rows from top to bottom: 2.5, 5, 10, 30, 60 and 240 min). The displayed channels are from left to right: surface topography, 1st order mechanical phase and 2nd order optical phase channels of scans collected at 1740, 1600, 1510 and 1100 cm-1 irradiation. Extracted line profiles for* sSNOM *signals obtained from PDA layers anchored on* Si/SiO_2, $N\text{-}TiO_x$ *and Au at ToD of 30 min.*

Conversely, on Au surfaces, aggregates coalesce into larger, more clustered domains. AFM topography and phase imaging further confirmed that substrate surface energy influences not only the size but also the lateral packing of PDA particles during early deposition.[100] Interestingly, the variability in chemical structure and morphology across substrates diminishes with longer deposition times. By approximately 240 min., far-field FTIR and XPS data suggest that the composition of the surface-confluent PDA layer becomes relatively uniform regardless of substrate. This observation supports the hypothesis that surface-specific effects dominate the early phase of film growth, but are eventually overwhelmed by solution-phase aggregation and bulk deposition dynamics.[99]

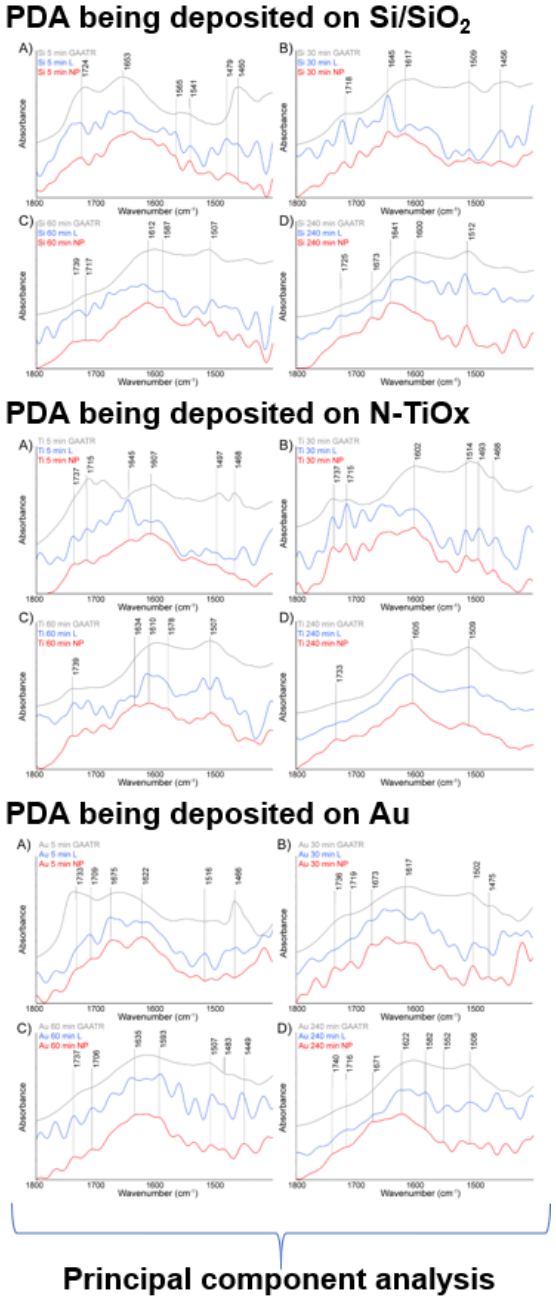

Fig. 10. *Comparison of nano-FTIR spectra of PDA layer (L) and nanoparticles (NP) with GAATR-FTIR spectra for Si/SiO$_2$, N-TiOx and Au substrates. The PDA deposition time was A) 5 min, B) 30 min, C) 60 min, and D) 240 min. The spectra are displayed on full scale and offset in the y-axis for maximum clarity. Nano-FTIR data was subjected to PCA analysis.*

The sSNOM analysis further confirmed that the substrate material significantly influences the nanoscale structure and chemical composition of PDA films. PDA growth was fastest on gold, where early and strong optical signals corresponding to indole (1510, 1600 cm^{-1}) and quinoid (1740 cm^{-1}) vibrations indicated rapid formation of chemically diverse PDA layers driven by π–π stacking and hydrophobic interactions (**Fig. 9**). In contrast, PDA growth on Si/SiO$_2$ and N-TiO$_x$ was slower and more uniform, with nanoaggregates forming later and weaker quinoid signals, reflecting a polymerization pathway dominated by coordination and hydrogen bonding. Across all substrates, the 1510 and 1100 cm^{-1} signals showed the strongest correlation with surface topography, highlighting chemical and structural differences between the continuous PDA layer and nanoaggregates.

We determined 30 minutes of deposition time (ToD) to be the representative crossover at which a significantly thick surface confluent PDA layer has adhered on the substrates. We used the term ToD as it is merely impossible to distinguish between the several concomitant processes leading to deposition of various intermediates, stacks and polymer chains and, at the same time, surface- initiated growth of a continuous surface adherent PDA layer and adsorption/adherence of nanoaggregates. We observed distinct differences in PDA film composition and morphology were across the three substrates using sSNOM. On Au substrates PDA showed the most advanced development, with clear optical signals at all key vibrational frequencies centered at 1510 cm^{-1} (indole), 1600 cm^{-1} (indole), and 1740 cm^{-1} (quinoid) indicating a chemically diverse and thicker PDA layer. This contrasts with Si/SiO$_2$ and N-TiO$_x$, where the 1740 cm^{-1} signal remained weak or absent, suggesting fewer quinoid intermediates at this stage. Additionally, optical phase contrast at 1510 and 1100 cm^{-1} correlated well with nanoaggregate topography on all substrates, but Au exhibited a greater number of distinct aggregates and stronger signal intensity, reflecting faster PDA growth. The differences underscore

how Au promotes more rapid and chemically varied PDA assembly, while oxide surfaces yield slower, more uniform layers with less pronounced intermediate content at 30 min ToD. At longer times of deposition (60 and 240 minutes), PDA films on all substrates showed increased thickness, surface roughness, and a higher density of nanoaggregates. The sSNOM data revealed stronger optical contrast at 1510 and 1100 cm^{-1}, corresponding to indole units and substrate interactions, with signals closely matching the topographical features of the aggregates. The 1740 cm^{-1} signal, associated with quinoid polymerization intermediates, became clearly detectable on SiO_2 and N-TiO_x only at these longer deposition times, whereas it was already apparent at earlier stages on Au, indicating a more abundant and sustained presence of intermediates on gold.

At longer ToD, nanoFTIR analysis showed negligible difference in the absorption profiles of PDA films formed on Si/SiO_2, N-TiO_x, and Au (***Fig. 10***). To handle the high-dimensional data produced by grazing angle attenuated total reflection FTIR and nanoFTIR, we have turned to principal component analysis (PCA) of spectral data and thus reduced complexity and identify clustering patterns in spectral datasets. PCA distinguished nanoaggregate spectra from confluent layer spectra, revealing tighter grouping of aggregate signals, pointing to greater molecular uniformity. Conversely, film spectra displayed broader distribution in PC space, reflecting chemical heterogeneity across the surface. PCA thus serves as a powerful tool for highlighting subtle spectral variations not easily observed by direct inspection. PCA analysis of nanoFTIR datasets further confirmed this convergence, with 240 minutes samples from all three substrates clustering closely in principal component space.[99]

To summarize, although PDA is capable of forming coatings on a wide variety of materials, its growth behavior and chemical properties are substrate-sensitive during the early stages of deposition. Understanding and harnessing this sensitivity allows for more precise control over film structure, enabling tailored surface functionality for advanced applications. In the next section, we explore the duality of PDA film structure, i.e. the simultaneous presence of a surface-confluent layer and nanoaggregates, and how their composition, morphology, and formation mechanisms differ.

1.3 Spectral Distinction Between Surface-Confluent PDA Layers and Nanoaggregates. [*D10, D13, D15-D17*]

One of the most intriguing findings in the study of PDA film formation is the coexistence of two structurally and possibly chemically distinct domains on the modified surface: (1) a uniform, surface-adherent PDA layer and (2) particulate nanoaggregates that adsorb on top of or alongside this layer. Though initially overlooked in earlier studies, our recent advances in high-resolution surface characterization, particularly sSNOM and nanoFTIR spectroscopy, have revealed that these two domains exhibit differences in their morphological and chemical profiles.

The surface-confluent PDA film begins as a thin seed layer formed by the direct interaction between oxidized dopamine species and the substrate. Over time, it grows through surface-initiated polymerization and lateral fusion of adsorbed oligomeric intermediates. This film is generally smooth (relative to the underlying substrate), continuous, and only modestly heterogeneous in composition. Ellipsometric thickness measurements indicate typical values ranging from 5 to 30 nm, depending on deposition time and substrate type.[12, 99] In contrast, PDA nanoaggregates form in solution during the oxidative polymerization process. These suspended particles nucleate and grow through self-assembly and π–π stacking of oligomers and then settle onto the substrate via sedimentation or random adsorption. Their formation appears to be largely substrate-independent but is significantly influenced by deposition time and dopamine concentration. AFM and sSNOM images demonstrate that the size, shape, and spatial distribution of these aggregates vary widely, with heights reaching up to 50–100 nm and lateral dimensions of several hundred nanometers.[12, 93, 99, 100] NanoFTIR spectroscopy enabled us to directly compare the chemical composition of nanoaggregates and the underlying film at the sub-100-nm scale. Measurements targeting key infrared bands, such as the C=O stretch of quinones (~1740 cm^{-1}), the C=C stretch of indoles (~1600 cm^{-1}), and the ring vibrations of catechols (~1510 cm^{-1}), reveal spectral shifts and intensity variations between aggregates and the surrounding matrix. In most cases, nanoaggregates showed stronger absorption at indole-specific bands and less pronounced quinone features, suggesting that the aggregates may be richer in cyclized dopamine units and more aromatic in nature.[99] Furthermore, aggregates displayed sharper and more intense vibrational bands, indicating a more homogeneous local composition. This contrasts with the broader, more complex absorption profiles of the surface

layer, which result from a mix of catechols, indoles, quinones, and other intermediates. PCA of nanoFTIR spectra confirms this distinction: while spectra from the surface layer exhibited wide distribution across PC space, the nanoaggregates spectra tightly clustered, implying higher chemical uniformity within aggregates.[99]

1.4. Functional implications and applications of PDA film architecture.

The detailed understanding of PDA film morphology and chemical structure, particularly the dual presence of a surface-confluent layer and nanoaggregates, has far-reaching implications for its utility across a wide range of disciplines. The inherent versatility of PDA, stemming from its abundant functional groups and universal adhesion properties, has enabled its use in diverse applications ranging from biosensing to antifouling coatings, drug delivery platforms, and surface-mediated cell signaling. The multifaceted structural and chemical behavior of PDA films revealed through a combination of macroscopic far-field spectroscopies and nanoscale spectroscopic imaging, and functional analysis lays the groundwork for a more systematic and rational approach to PDA surface engineering. Rather than treating PDA as a monolithic, universally applicable coating, it becomes increasingly important to view it as a modular and tunable interface, whose properties can be controlled through deposition conditions, substrate selection, and post-processing.

Chapter 2 – Macromolecular and biofunctionalization approaches for the synthesis of polymer brushes.

The undesired adsorption of proteins, cells, and microorganisms on material surfaces, often termed as fouling, is a critical challenge in the development of biomaterials and biointerfaces. This phenomenon occurs rapidly upon exposure of artificial material surfaces to biological fluids and can initiate a cascade of adverse events such as inflammation, thrombosis, immune reactions, and biofilm formation. To mitigate these effects, non-fouling polymer coatings composed of polymer brushes have become an indispensable tool across a wide range of biomedical applications, including implants, biosensors, and drug delivery systems.

2.1 "Grafting-to" approach for the synthesis of polymer brushes. [*D2, D9, D11-D13, D18-D22*]

Among the methodologies developed for creating antifouling surfaces, the "grafting-to" approach stands out for its operational simplicity, reproducibility, and structural versatility. In "grafting-to", pre-synthesized polymer chains bearing reactive end groups are covalently attached to substrates. This strategy enables the direct application of well-characterized polymers with defined molar mass, composition, and architecture. This is particularly advantageous when the goal is not only to resist fouling but also to introduce bioactive or bioresponsive functionalities, such as cell-adhesion ligands, imaging agents, or stimuli-sensitive moieties.[10-12, 102] Compared to "grafting-from" approaches, where polymers are grown in situ from surface-anchored initiators, the grafting-to approach allows complete pre-characterization of the polymer prior to immobilization. However, a well-known limitation of the "grafting-to" method is the volume steric exclusion effects that occurs as surface coverage increases, restricting the attainable grafting density. As polymer chains attach, they physically block nearby reactive sites, leading to a plateau in brush thickness and density. These limitations, however, can be partially overcome by strategies such as the use of poor solvent conditions to shrink polymer coil size during attachment. [9, 10, 89] By canceling out the presence of solvent and performing the grafting from melt we have managed to maximize the grafting density of PEO chains.[10-12, 18, 102]

The antifouling properties of polymer brushes derive primarily from two energetic penalties that oppose protein adsorption. The first is an enthalpic barrier caused by the need to displace tightly bound water molecules from the hydrated polymer layer, which is energetically costly. The second is an entropic barrier arising from the compression of densely packed chains, which resist deformation as proteins approach. These effects are maximized when the grafting density is high enough to enforce the polymer chains to stretch into a brush regime (i.e., $D/2R_g < 1$) as a result of the strong interchain overlapping.[11, 12, 89]

Despite stated constraints, the "grafting-to" technique has shown outstanding utility in creating multifunctional coatings that combine antifouling resistance with bioactivity or responsiveness. For example, poly(ethylene oxide) (PEO), poly(2-oxazoline)s (PAOx), poly(2-oxazine)s (PAOzi), poly[*N*-(2-hydroxypropyl)methacrylamide] (PHPMA), and poly[*N*-(2-fluoroethyl)acrylamide] (PFEAM) have

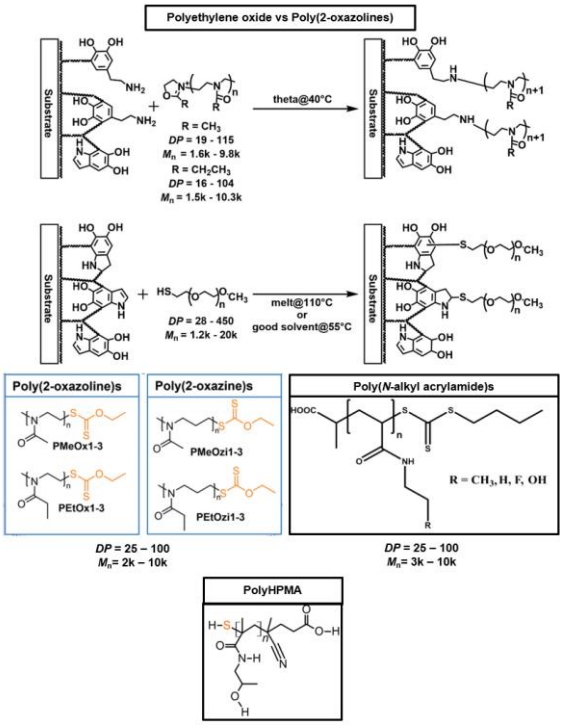

Fig. 11. *Schemes presenting developed library of polymers used for the synthesis of polymer brushes via the "grafting-to" approach.*

all been successfully employed in grafting-to configurations (***Fig. 11***). [9, 65, 103] These polymers differ in flexibility, hydrophilicity, and chemical reactivity, enabling their selection and tailoring for specific applications. Notably, PFEAM exhibits dual-functionality, providing both high fouling resistance and fluorine visibility for ^{19}F MRI tracing and imaging.[65, 104]

In the context of bioactive coatings, grafting-to allows modular functionalization. Bioactive motifs such as peptides can be incorporated into polymer chains after grafting via highly specific "click" chemistry reactions, preserving their biofunctionality during surface attachment. Such design enables precise control over ligand density, spatial distribution, and orientation, which are identified as key factors that regulate cell adhesion, spreading, and differentiation.[10, 18, 102] In summary, the grafting-to technique provides a versatile and chemically precise method for engineering antifouling and biofunctional polymer brushes. Its simplicity and compatibility with pre-functionalized polymers make it especially suited for creating multifunctional surfaces where bioactivity and antifouling performance must coexist. Although inherently limited in ultimate grafting density, continued innovations in polymer architecture, solvent engineering, and surface chemistry are broadening the applicability of grafting-to strategies in biomaterials science and nanomedicine.

2.1.1. Polymers used in "grafting-to": from PEO to fluorinated alternatives. [*D11-D13, D18-D20, D23*]

The choice of polymer is a central factor in determining the antifouling performance of grafting-to coatings. While PEO has long been the gold standard for hydrophilic, non-fouling surfaces, its limitations (such as immunogenicity and possible oxidative instability) have driven the development of alternative polymer systems. In grafting-to strategies, several next-generation polymers have demonstrated superior performance: PAOx, PAOzi, PHPMA, and the recently developed PFEAM. Poly(2-alkyl-2-oxazoline)s, particularly poly(2-methyl-2-oxazoline) (PMeOx) and poly(2-ethyl-2-oxazoline) (PEtOx), are amphiphilic, nonionic polymers synthesized by cationic ring-opening polymerization. They exhibit excellent water solubility and low toxicity, making them strong candidates for biocompatible antifouling surfaces. In direct comparisons with PEO of similar molar mass and surface thickness, PMeOx consistently showed lower protein adsorption from human blood plasma. We confirmed this across a range of degrees of polymerization (DP = 16 – 115), using PDA as the anchoring layer, where PMeOx coatings achieved higher grafting densities and stronger suppression of protein adsorption than PEO under matched surface-related parameters.[9] The antifouling efficacy of PAOx brushes is closely linked to their hydrophilicity and packing conformation. While both PMeOx and PEtOx form effective brushes, PMeOx, with its shorter side chain, demonstrates better hydration and thus greater enthalpic resistance to protein adsorption. The effective suppression of fouling by PAOx coatings is further amplified by their brush-like structure when grafted at densities above 0.2 chains/nm², with conformational data indicating extended chains in the aqueous phase.[9]

Poly(2-alkyl-2-oxazine)s (PAOzi), exemplified by poly(2-ethyl-2-oxazine) (PEtOzi), have emerged as a superior subclass of polymers due to their increased backbone flexibility and lower glass transition temperature. When grafted-to gold surfaces using thiol-reactive xanthate-functionalized ends, PEtOzi brushes demonstrated the best antifouling properties among all tested polymers, including PEO, PMeOzi, PMeOx, and PEtOx. Despite their moderate hydrophilicity, the flexibility of

the PAOzi backbone enables greater swelling and higher water content per monomer unit, as confirmed by ellipsometry and water uptake measurements. This enhances the enthalpic barrier to fouling, making PEtOzi the most effective of the tested series in resisting adsorption from complex biological media like human blood plasma.[9, 103]

PHPMA is another neutral, hydrophilic polymer known for its biocompatibility. Over the past few decades this polymer has become the silver bullet of drug-delivery platforms, while rarely employed in surface modification. We have utilized the “grafting-to” approach, to achieve PHPMA brushes which suppressed protein fouling from fibrinogen and serum albumin by more than 95%. However, when compared to their grafting-from analogs synthesized via surface-initiated ATRP and RAFT polymerization, PHPMA coatings prepared via the “grafting-to” approach consistently yielded lower thickness and grafting density resulting in lower antifouling performance. Still, PHPMA coatings prepared by “grafting-to” approach resisted non-specific adsorption from blood plasma to ~81 – 89%. This positions them as a solid performer for applications where simple anchoring procedures and moderate brush thickness is preferred.[89]

PFEAM represents a recent innovation in antifouling polymer design. Its backbone, derived from acrylamide, incorporates fluorinated side chains that create both hydration and fluorine-mediated protein repulsion effects. PFEAM chains were grafted onto gold surfaces via RAFT-derived trithiocarbonate end groups. Despite having thin dry layers (about 1.5 nm), PFEAM coatings reduced blood plasma fouling by over 90%, outperforming PEO layers of comparable thickness and structure. Importantly, PFEAM also introduces functionality for ^{19}F magnetic resonance imaging (MRI), enabling dual-use coatings for bioinertness and noninvasive tracing of coated devices or nanocarriers.[103]

The gained knowledge led to the development and systematic evaluation of a library of water-soluble fluorinated copolymers based on poly[(*N*-(2,2,2-trifluoroethyl)acrylamide)-stat-(*N*-(2-hydroxyethyl)acrylamide)], poly[(*N*-(2,2,2-trifluoroethyl)acrylate)-stat- (2-hydroxyethyl acrylate)]**,** poly[(*N*-(2,2,2-trifluoroethyl)acrylamide)-stat-(*N*-(2,3-dihydroxypropyl)acrylamide)], poly[(*N*-(2,2,2-trifluoroethyl)acrylamide)-stat-(tris(hydroxymethyl)methylacrylamide)]**,** poly[(*N*-(2,2,2-trifluoroethyl)acrylamide)-stat-(carboxybetaine acrylamide)]**,** poly[(*N*-(2,2,2-trifluoroethyl)acrylamide)-stat-(2-(methylsulfinyl)ethyl acrylamide)]**,** poly[(*N*-(2,2,2-trifluoroethyl)acrylamide)-stat-(*N*,*N*-dimethylacrylamide)], poly[(*N*-(2,2,2-trifluoroethyl) acrylamide)-stat-(*N*-acryloylmorpholine)], poly[(*N*-(2,2-difluoroethyl)acrylamide)-stat-(*N*-(2-hydroxyethyl)acrylamide)], and poly[(*N*-(2-((2,2,2-trifluoroethyl)sulfinyl)ethyl)acrylamide)-stat-(N-(2-hydroxyethyl)acrylamide)]. The synthesized library of statistical copolymers based on using various combinations of fluorinated monomers and hydrophilic comonomers, focusing on optimizing fluorine content**,** water solubility, magnetic relaxation**,** and signal-to-noise ratio (SNR)**.** Optimized copolymer poly[(*N*-(2,2,2-trifluoroethyl)acrylamide)$_{60}$-stat-(*N*-(2-hydroxyethyl)acrylamide)$_{40}$] (poly(TFEAM$_{60}$-*stat*-HEAM$_{40}$), exhibited higher ^{19}F sensitivity, greater design flexibility, and in vivo tumor imaging capability not only whithin the studied library but also in respect to PFEAM homopolymer. The optimized structure demonstrated superior detection limit vs PFEAM (< 1 mg/mL vs. 2.5 mg/mL, respectively), better SNR provided by the higher content of fluorine atoms within the structure, while preserving *in vivo* functionality, biocompatibility and antifouling properties (restricting the fouling by more than 80% in comparison to unprotected gold surfaces).

In summary, while PEO laid the foundation for the synthesis and understanding the physical-chemical origins of antifouling, the emergence of PAOx, PAOzi, PHPMA, and PFEAM has significantly expanded the toolbox for the design of non-fouling surfaces via the “grafting-to” method. Among these, PAOzi, especially PEtOzi, currently offers the most effective protein resistance, followed closely by PMeOx and PFEAM. Each polymer class presents unique advantages: PAOx for synthetic tunability and hydrophilicity; PAOzi for flexibility and hydration; PHPMA for biocompatibility and accessibility; and PFEAM for multifunctionality when *in vivo* tracing and imaging applications are in question. The selection among these depends on the specific performance and functional requirements of the target application.

2.1.2. Physical-chemical structure and characterization of polymer brushes synthesized by “grafting-to” approach. *[D2, D11, D13, D14, D18-D21, D23-D25*]

The performance of antifouling polymer brushes synthesized by “grafting-to” approach depends on not-only on the chemical structure defined by the monomer units but also on their

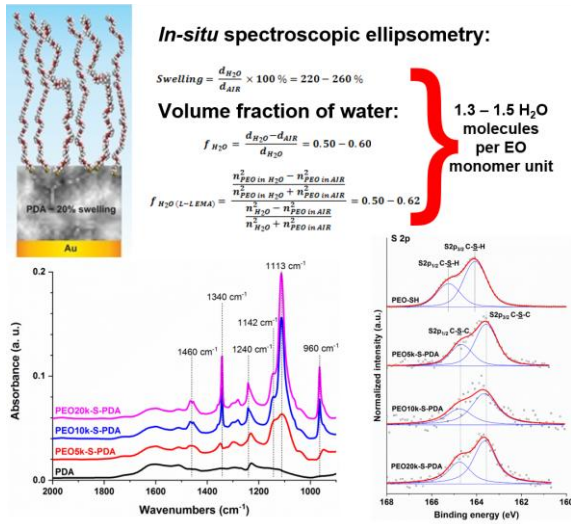

Fig. 12. *Schemes presenting developed library of polymers used for the synthesis of polymer brushes via the "grafting-to" approach.*

physical/conformational structure and how this influences the interfacial interactions with biological media. Key structural parameters include the grafting density (σ), dry and swollen brush thickness, chain conformation, and the degree of brush hydration (***Fig. 12***). Effective antifouling behavior typically emerges when polymer chains are densely packed enough to stretch away from the surface, known as the "brush regime". This is characterized by a $D/2R_g$ ratio below 1, where D is the distance between chains and R_g is the polymer radius of gyration.[10-12, 65, 89, 103-105]

Spectroscopic ellipsometry is commonly used to quantify both dry and hydrated film thicknesses, enabling calculations of swelling ratios ($SR = h_{swollen}/h_{dry}$) and number of water molecules per monomer unit. High swelling ratios indicate enhanced hydration, which contributes to the enthalpic barrier against protein adsorption. For instance, brushes based on PAOzi, particularly PEtOzi, exhibit *SR* of about 3.1–3.8 and [H_2O]/[M] ratios of 13–14. This indicates significant water retention within the swollen layers of PAOzi in comparisson to their PAOx analogues exhibiting *SR* of 2.3–2.6 and [H_2O]/[M] ratio of 6–7. This most probably originates from the higher flexibility of the PAOzi chains in comparison to PAOx.[103] PHPMA brushes also show variable swelling ratios which are dictated by maximum grafting density achieved within particular grafting conditions. Thus PHPMA layers synthesized via "grafting-to" avenue exhibit *SR* of 6.5 and 4.1 as a result of their lower chain stretching in the initial dry state for brushes formed under "good solvent" and "poor solvent" conditions.[89] We determined a *SR* in the range of about 2.0–2.8 for densely packed PEO brushes of various molar mass, further proving the high stretching of the brushes even in the dry state.[11]

Contact angle goniometry is another method to probe the interaction of polymer brushes with water. Hydrophilicity of polymer-coated surfaces (with lower angles indicating higher water affinity) is usually correlated with better antifouling potential of the brushes. Across our studies, polymer brush coatings performed via the "grafting-to" approach with hydrophilic functional groups, such as hydroxyl (PHEAM, <10°), ether (PEO, 12–17°), and fluoroethyl (PFEAM, ~27°)exhibited the lowest contact angles and strongest resistance to protein adsorption. In contrast, less hydrophilic coatings like PPAM (~60°) and PEAM (~41°) showed higher contact angles and weaker antifouling performance.[10-12] Poly(2-oxazoline)s and poly(2-oxazine)s also showed excellent hydrophilicity: PMeOx and PMeOzi brushes had contact angles of 12° and 20°, respectively, while PEtOx and PEtOzi exhibited less pronounced hydrophilicity with contact angles of 33° and 39°.[9, 103] Increasing polymer chain length of PEO generally enhanced hydrophilicity, and substrates with dense polymer brushes (especially those formed from melt or with polar side groups) demonstrated significantly lower contact angles, serving as a prerequisite for improved antifouling effectiveness.[10-12]

XPS and reflection modes of FTIR analyses such as grazing angle attenuated total reflection and reflection absorption spectroscopies (GAATR-FTIR and IRRAS) have been instrumental in characterizing the chemical structure of the PEO, PAOx, PAOzi, (meth)acrylate and (meth)acrylamide based polymer chains (***Fig. 12***).[9, 11, 12, 86, 103] We have utilized high-resolution XPS analysis of the C 1s, N 1s, O 1s, F 1s, etc. regions and spectral deconvolution to determine the attained covalent structure of the brushes. Notably, by analysis of atoms present in the anchoring moieties, such as sulfur and high-resolution XPS analysis of S 2p region, enabled the verification of the covalent anchoring of the polymer chains through thiol, disulfide, xanthate, preserved-CTA groups on polymers synthesized via RAFT, such as dithiocarbonate, and trithiocarbonate.[86, 89, 103, 105, 106] The chain-end C–S–H groups of PEO chains of various molar

mass give the dominating S $2p_{3/2}$–S $2p_{1/2}$ spin split doublet with the major S $2p_{3/2}$ and minor S $2p_{1/2}$ contributions centered at about 164.1 eV and 165.2 eV, respectively. The presence of the chain-end groups of PHPMA i.e. C–S–H moieties (achieved after aminolysis of the CTA groups) give the dominating S $2p_{3/2}$–S $2p_{1/2}$ spin split doublet with the major S $2p_{3/2}$ and minor S $2p_{1/2}$ contributions centered at about 163.8 eV and 164.7 eV, respectively. The covalent binding of the PEO chains bearing thiol end-groups to PDA was verified by shifts in the binding energies of the S $2p_{3/2}$–S $2p_{1/2}$ doublet (to respective values of about 163.6 eV and 164.7 eV, respectively) characteristic for the established C-S-C bonding. The covalent binding of the poly(HPMA) chains bearing thiol end-groups to gold was verified by shifts in the binding energies of the S $2p_{3/2}$–S $2p_{1/2}$ doublet (to respective values of 161.8 eV and 163.2 eV, respectively) characteristic for the established C-S-Au thiolate bonding. The high-resolution XPS spectra taken in the S 2p region of free polymers bearing the trithiocarbonate chain ends show a rather broad spectral feature of the expected C–S–C(=S) and C–S–C(=S) moieties. The C–S–C(=S) moieties give the dominating S $2p_{3/2}$–S $2p_{1/2}$ spin split doublet with the major S $2p_{3/2}$ and minor S $2p_{1/2}$ contributions centered at 163.9 eV and 165.1 eV, respectively. The C=S moiety gives the rise of the shoulder contribution with a S $2p_{3/2}$–S $2p_{1/2}$ spin split doublet with the major S $2p_{3/2}$ and minor S $2p_{1/2}$ contributions centered at 162.7 eV and 163.9 eV, respectively. The ratio between the C–S–C(=S) and C=S moieties represents well the expected theoretical ratio within the C–S–C(=S)–S–C thrithiocarbonate group of 2 : 1. The covalent grafting of the polymer chains bearing the trithiocarbonate chain to gold leads to a shift in the major S $2p_{3/2}$ and minor S $2p_{1/2}$ contributions of the doublet to the lower binding energy of about 161.7 eV and 163.0 eV, respectively, which is proved the established C–S–Au bonds.

Furthermore, the IRRAS has been used to probe the conformation and orientation PEO brushes (***Fig. 12***). IRRAS studies of PEO brushes grafted to PDA revealed distinct C–O–C stretching bands near 1119 cm^{-1} and a sideband at 1151 cm^{-1}, which are sensitive to chain conformation and crystallinity. IRRAS measurements on PEO brushes end-tethered to polydopamine or on PLA substrates via PLLA-b-PEO block copolymers showed similar C–O–C vibrational bands at 1117–1120 cm^{-1} and 1343 cm^{-1}, attributed to helical conformations of PEO chains oriented perpendicular to the surface, thus hallmarking of a true brush state.[107] These spectral features became more prominent with increasing molecular weight of PEO, confirming improved brush ordering and hydration. Collectively, IRRAS findings confirm that PEO chains in these systems adopt a brush-like, often crystalline or semi-crystalline structure, and that their hydration state and orientation can be reliably monitored through well-defined vibrational bands. VSFG spectroscopy, a pump-probe technique sensitive to molecular vibrations at interfaces, further revealed critical insights into the molecular orientation and structural order of PEO brushes anchored to surface confluent PDA-modified surfaces and bare gold (***Fig. 13***).[11] In air, VSFG spectra showed strong CH_2 vibrational features attributed to *t+g−g* conformers within the polymer backbone, suggesting a partially helical, brush-like structure with methylene groups oriented toward the substrate. The methoxy end groups, however, exhibited no significant VSFG signal, indicating random orientation. Upon immersion in water, PEO brushes exhibited significant hydration and conformational disorder, particularly in amine-tethered (PEO-N(H)-PDA) films, which became nearly VSFG inactive. In contrast, thiol-tethered brushes (PEO-S-PDA and PEO-S-Au) retained weak but discernible signals, especially from *+g+g−g* conformers near the

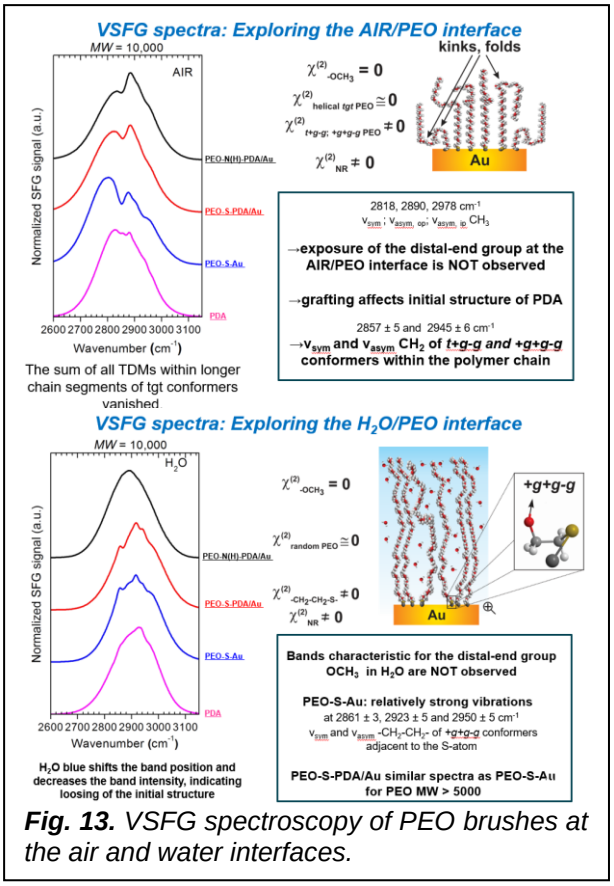

Fig. 13. *VSFG spectroscopy of PEO brushes at the air and water interfaces.*

anchoring site, suggesting some preserved order close to the substrate.[11] Higher molecular weight PEOs showed increased swelling and disorder, yet also contributed to higher local order near the surface. These findings highlight how tethering chemistry and polymer length influence interfacial organization and hydration behavior. VSFG's surface specificity complements bulk-sensitive IRRAS results, together confirming that PDA-tethered PEO layers can achieve brush-like conformations while maintaining hydration-induced flexibility. This balance of structural order and dynamic behavior underpins their excellent protein-repellent properties and versatility for biomedical surface modification.

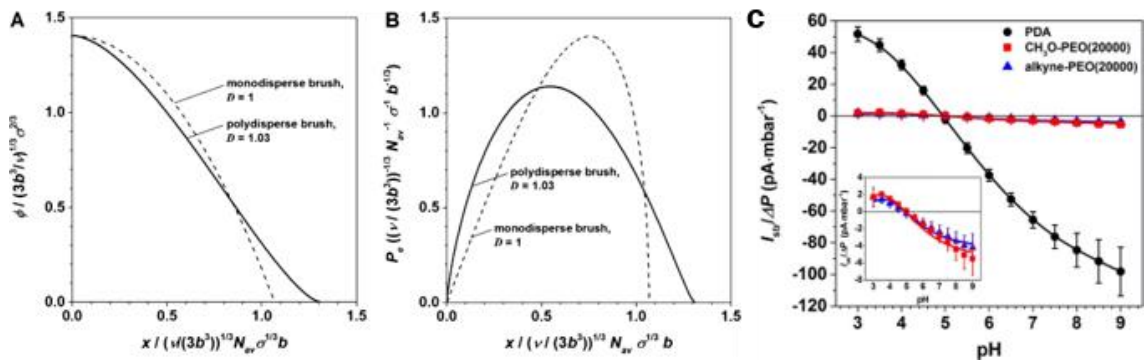

Fig. 14. *Density profile (A) and chain end distribution (B) for PEO brushes with a dispersity Đ = 1.03 and monodisperse brushes (Đ = 1) in rescaled units. Streaming current over applied pressure, $I_{str}/\Delta P$, as a function of pH in 1 mM KCl solution for the PDA layer (black) as well as the PDA layer after immobilization of CH_3O−PEO(20 000) (red) and alkyne−PEO(20 000) (blue) brushes. Experimental data are represented as symbols, and the solid lines represent simulation results. For further information refer to D14.*

Electrokinetic studies of PEO brushes reveal their strong capability to screen underlying substrate charge and resist protein adsorption due to their dense, hydrated polymer structure.[10, 108-110] Streaming current measurements, combined with self-consistent field theory, effectively capture the brush's segment density distribution, including the gradual tailing in polydisperse systems, which are hard to be resolved even when employing methods like neutron reflectivity (***Fig. 14***). The brushes exhibit low to near-zero zeta potentials across a range of pH and ionic strengths, attributed to both the hydrodynamic exclusion of flow within the brush and preferential adsorption of water ions (OH^- > H_3O^+) at the substrate. The hydrodynamic penetration depth into the brushes is shallow (~15–20 nm), further contributing to the electrostatic shielding.[10] These features confirm that PEO brushes, especially at moderate to high grafting densities, form an electrostatically neutral interface ideal for biomedical and surface engineering applications.

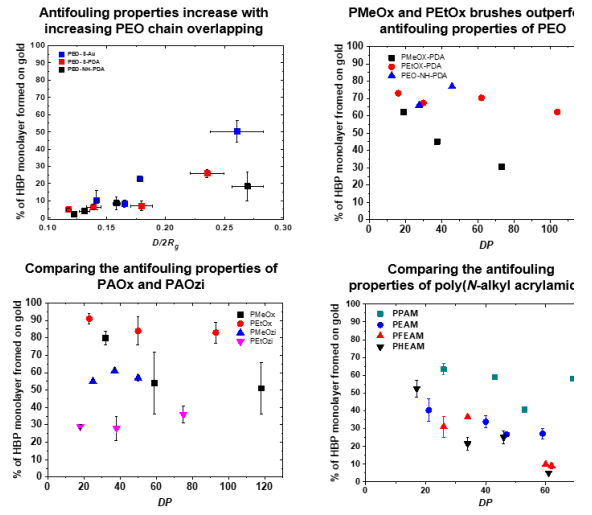

Fig. 15. *Comparison of antifouling properties of various polymer brushes synthesized via the "grafting-to" approach.*

2.1.3 Comparative antifouling performance of polymer brushes synthesized by "grafting-to" approach. [*D2, D11-D13, D18-D21, D23*]

Systematic comparisons across different polymer types and architectures have demonstrated that the antifouling performance of grafting-to brushes strongly depends on both polymer chemistry and physical structure (***Fig. 15***). Grafted PEO brushes typically reduce fibrinogen and albumin adsorption by ~90%, although their performance declines with increasing chain length due to reduced grafting density and adsorption in sparse regions.[9] Indeed our efforts showed that as high as 98% reduction of fouling can be achieved by densely packed PEO brushes obtained through the melt "grafting-to" avenue. However, recent identification of PEO-specific immunoglobulins, has shifted the spotlight in

search of new antifouling materials and polymers capable of withstanding these detrimental effects. Brushes formed from PAOx (PMeOx and PEtOx) significantly outperform PEO analogs under matched surface-related parameters. In one study, PMeOx brushes with DP ~6k reduced fouling from whole plasma to ~30% relative to bare gold, with superior performance attributed to the balance of flexibility, hydration, and short side chains.[9] PAOzi brushes, especially PEtOzi, achieve >70% resistance to protein fouling from blood plasma, largely due to their highly flexible backbones, low T_g, and high-water content, which jointly enhance both enthalpic and entropic barriers.[103] In contrast, poly(HPMA) brushes performed via "grafting-to" under optimized solution quality reach higher antifouling behavior. These PHPMA brushes managed to suppress the fouling from blood plasma up to ~81% and ~89% in comparison to unprotected gold when the "grafting-to" reaction was performed under good and poor (cloud point) conditions.[89] Understandably, "grafting-from" methods yield denser and more extended brushes, achieving even complete suppression of fouling.[89] Interestingly, our studies found PFEAM (semifluorinated yet hydrophilic polymer) brushes also show remarkable antifouling efficacy, achieving >90% reduction in plasma fouling. Their performance is enhanced by the presence of fluorine atoms that repel proteins and strengthen hydration shells, while also enabling ^{19}F MRI visibility, positioning PFEAM as a dual-functional antifouling and imaging platform.[65, 104, 105]

2.1.4. Functional implications and applications of polymer brushes synthesized via the "grafting-to" avenue.

The grafting-to method offers a structurally controlled, reproducible, and chemically flexible route to fabricating antifouling polymer brushes. Despite its inherent limitations in achieving high thicknesses and very high grafting densities, it remains a preferred method when precise molecular design of surface parameters, orthogonal functionalization, or combined antifouling and bioactivity is needed. Future optimization will likely focus on enhancing grafting densities through techniques like poor-solvent grafting and thermal annealing. Polymer classes like PAOx, PAOzi, polyacrylamides (PHEAM, PFEAM) and polymethacrylamides (PHPMA) already demonstrate that exceptional antifouling performance is achievable through an optimized "grafting-to" anchoring. The integration of stimuli-responsiveness, bioactive ligands, or imaging modalities into brush structures is a rapidly evolving frontier. Analytical techniques such as nanoFTIR and sSNOM will continue to shed light on subtle yet critical variations in brush structure, guiding the next generation of autonomous surface coatings. With continued innovation, "grafting-to" strategies can meet the growing demands of precision medicine, implantable diagnostics, and regenerative interfaces.

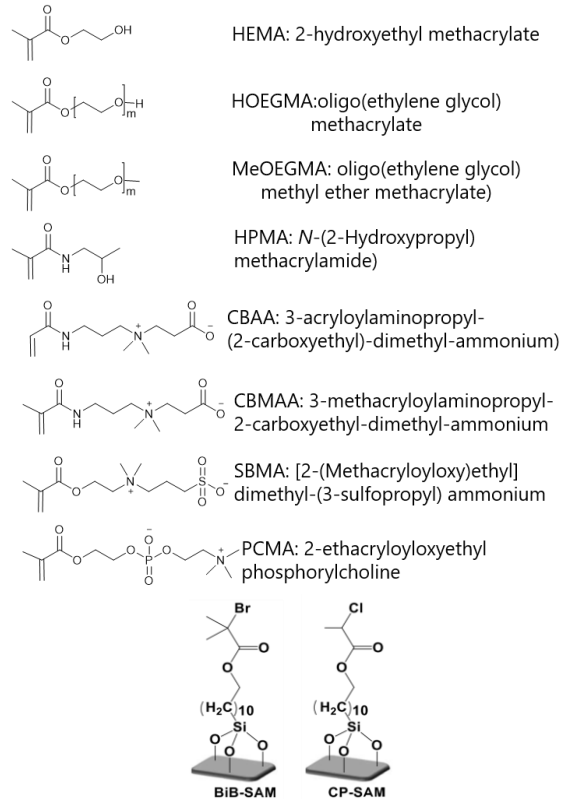

Fig. 16. *Hydrophilic monomers and initiator SAM's used for SI polymerizations. The Br moiety can be exchanged for a CTA moiety through a radical mechanism. Surface anchoring can be adjusted.*

2.2 "Grafting-from" approach for the synthesis of polymer brushes. [*D1, D6, D26-D38*]

By employing the "grafting-from" approach, through employing surface-initiated polymerization, we circumvent the steric constraints which are inherent to the "grafting-to" method. This is achieved by growing the polymer chains in situ from initiator sites immobilized on the substrate's surface. The monomer diffuses freely from solution to the surface, where propagation proceeds from each initiator point. This strategy enables high grafting densities and extended chain lengths, producing well-defined brush conformations characterized by chain stretching perpendicular to the surface. This contrasts with

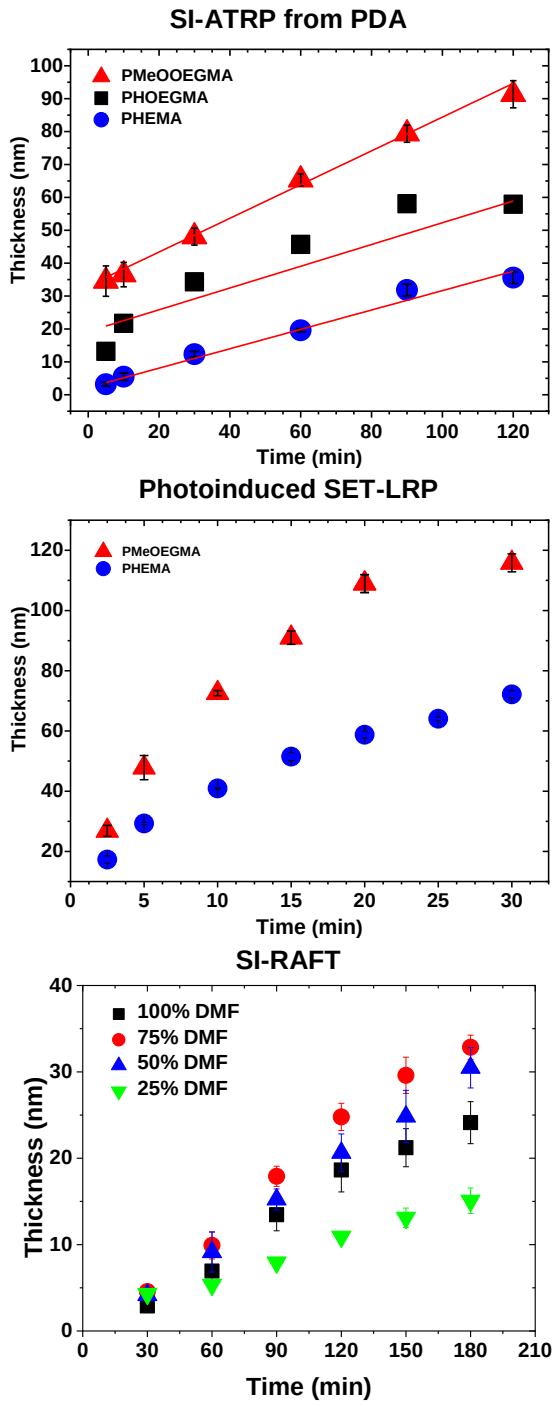

Fig. 17. *SE measurements of polymer brush thickness pointed to attained "macroscopic" control over the SI-ATRP, photoinduced SET-LRP and SI-RAFT polymerizations.*

"grafting-to" approach, where film thickness is limited by the diffusion barrier formed by pre-grafted chains. Consequently, "grafting-from" yields polymer brushes with significantly enhanced antifouling characteristics due to the formation of a highly hydrated, entropically resistant interfacial barrier. Through the employment of controlled surface-initiated polymerization methods such as SI-ATRP, photo-SET-LRP and SI-RAFT, we have managed to synthesize a wide range of polymer brushes of different chemical structure (**Fig. 16** and **Fig. 17**) and architecture, i.e. lateral and vertical structuring. The employment of controlled radical polymerizations offers fine control over brush composition and architecture, enabling the synthesis of block copolymers. The preserved structure of the halide and CTA end-groups can be inferred from the attained controlled kinetics, but also from re-initiation experiments. The presence of these moieties can be directly inferred from the XPS measurements, although in cases of thin polymer brushes it is merely impossible to distinguish between moieties that did not initiate the SI-polymerization and the ones that are present on the "living" polymer chain-ends.

Preserved chain ends can be utilized for the direct modification and enrichment of the brushes with functionalities suitable for "click" chemistry reactions. CP enabled the synthesis of polymer brushes with chemically distinct segments arranged along the *z*-axis providing the possibility of tuning the material properties for controlled wetting, fluorescence-based sensors, immobilization of biorecognition elements for the detection of analytes in biosensing applications, or the synthesis of bioactive polymer brushes bearing ECM mimetic peptides.[10, 13, 20-23, 102, 111-113] These features point to the applicability of the developed avenue for the hierarchical encoding of envisaged autonomous surface. Even more, as polymerization can be spatially triggered by light or localized by catalyst patterning/delivery, grafting-from techniques facilitate lateral surface structuring at micro- and nano-scale resolution, making them well-suited for applications that require discrete functional domains like biosensing and tissue-engineering.[67, 114, 115]

Despite its benefits, the "grafting-from" method presents several practical and mechanistic challenges. Understandably, the "grafting-from" method concerns synthetic complexity as it requires precise surface functionalization with initiator monolayers and often controlled inert atmospheres for polymerization. Some monomers are very sensitive to polymerization conditions. In aqueous SI-ATRP, acrylamide monomers (e.g., HEAm, FEAm) present challenges such as catalyst deactivation or side reactions (e.g., halide exchange, possible nucleophilic substitution), requiring optimization of initiators (e.g., CP vs. BiB) and halide

sources.[88, 116] This makes the method more technically demanding compared to “grafting-to”, which uses well-characterized polymer chains that can be coupled under less stringent conditions.

2.2.1. Monomers used in “grafting-from”: The toolbox for achieving diverse architectures. [*D1, D2, D6, D26-42*]

We successfully utilized CPs of various monomers (***Fig. 16***) including styrene, acrylate-based (such as methyl acrylate (MA), 2-hydroxyethyl acrylate (HEA), 3-(dimethylamino)propyl acrylate (DAPA), oligo(ethylene glycol) methyl ether acrylate (MeOEGA), n-butyl acrylate (nBA), 2-ethylhexyl acrylate (EHA), [2-(acryloyloxy)ethyl]trimethylammonium chloride (AETMAC), t-butyl acrylate (tBA)), N-hydroxysuccinimidyl methacrylate (MSI), methacrylate-based (oligo(ethylene glycol) methyl ether methacrylate (MeOEGMA), oligo(ethylene glycol) methacrylate (HOEGMA), 2-hydroxyethyl methacrylate (HEMA), 2-hydroxypropyl methacrylate (HPM), 2-(dimethylamino)ethyl methacrylate (DMAEMA), glycydyl methacrylate (GMA), t-butyl methacrylate (tBMA), n-butyl methacrylate (nBMA), methyl methacrylate (MMA), 2-ethylhexyl methacrylate (EHMA), isobornyl methacrylate (IBMA), solketal methacrylate (SMA)), acrylamide-based (carboxybetaine acrylamide (CBAA), *N*-(2-fluoroethyl)acrylamide (FEAM), *N*-(2-hydroxyethyl)acrylamide (HEAM)), methacrylamide-based (carboxybetaine methacrylamide (CBMA), HPMA), 2-isopropenyl-2-oxazoline (IPOx) for the synthesis of polymer brushes of diverse chemical composition.[19, 21-23, 66, 67, 89, 90, 113, 117-119] We further utilized the toolbox for the synthesis of various surface confluent architectures of homopolymer, random copolymer and block copolymer brushes with the possibility of obtaining laterally statistically organized or precisely patterned surfaces.

2.2.2. Physical-chemical structure and characterization of polymer brushes synthesized by “grafting-from” approach. [*D1, D8, D31-D35*]

The “grafting-from” approach produces brushes of high grafting density and tunable thickness, essential for antifouling applications due to their capacity to form dense protein-repellent interfacial layers. [88] The polymer chains can grow to tens or even hundreds of nanometers in thickness due to controlled chain propagation. The rate of propagation of SI-ATRP $R_{p\,(SI\text{-}ATRP)}$ is directly proportional to the rate of the increment of the thickness (d*h*/d*t*) of the brush (**Fig. 17**). During a surface-initiated and surface-confined process the concentration of monomer [M], catalyst [Cu(I)] and [Cu(II)] remain constant due to their huge excess compared to the initiating sites at the surface. Therefore the increment of thickness is directly proportional to the number of growing chains [P_n-X]. Thus, it can be used to assess achieved control of polymerization process. A linear increase in the brush thickness with polymerization time indicates a constant rate of propagation and therefore a constant number of “living” centers. Thus, through the measurement of the thickness we proved achieved control of the polymerization during the SI-ATRP of a wide range of monomers. Furthermore, SE measurements of polymer brush thickness pointed to attained “macroscopic” control over the photoinduced SET-LRP and SI-RAFT processes. This further underlines the well-controlled polymerization kinetics of the brushes, enabling the tuning of the surface adherent architectures at a nanometer scale. Even more, the optimized SI-ATRP, SET-LRP and SI-RAFT conditions can be directly adopted for the modification of a range of surfaces as proven through the immobilization of initiating molecules on PDA anchoring layers. This extends the concept of non-fouling brushes synthesis via the “grafting-from” avenue to virtually any solid surface providing an asset toward autonomous surfaces.

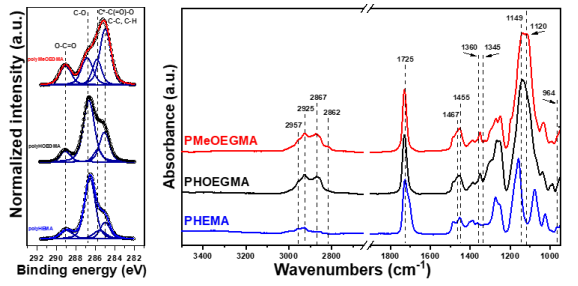

Fig. 18. *Example of XPS and IRRAS analysis of PMEOGMA, PHOEGMA and PHEMA polymer brushes synthesized via the “grafting-from” approach.*

Characterization of the covalent structure and surface properties of such brushes begins with precise determination of the initiator/chain transfer agent monolayer thickness and presence of characteristic groups. As in the case of “grafting-to” approach, spectroscopic ellipsometry is used to probe the thickness of the polymer brushes synthesized via the “grafting-from” approach. However, due to the inherent properties of preparation method and the unknown molar mass and dispersity of polymer chains, it is rather demanding to directly determine/derive the surface parameters of the polymer brushes, such as

grafting density, distance between grafting sites, D/R_g, etc. XPS and reflection modes of FTIR (GAATR-FTIR and IRRAS) confirm the expected binding environments and chemical functionalities—such as C–O, C–F, C–N, C(=O)–NH amide, C(=O)–O ester, C(=O)–O–H carboxy and C–O–H hydroxy groups—in polymer brushes based on previously elaborated monomers (***Fig. 18***). In the verification of the obtained chemical structure a we put a particular accent in the precise determination of the ratios between observed XPS spectral contribution and their relation to the theoretical values expected from the monomer composition. We utilized FTIR analysis to further strengthen XPS findings on the chemical structure of obtained polymer brushes and even through considerations about the polarization selectivity of GAATR-FTIR and IRRAS to probe the orientation of the polymer brushes.

As previously noted, contact angle goniometry plays a pivotal role in evaluating the surface energy and hydrophilicity of polymer-modified materials, which are considered as critical determinants of their antifouling performance and biocompatibility. Across our studies, lower water contact angles consistently indicated higher surface energy and enhanced hydrophilicity of the brushes synthesized via “grafting-from”, one of key attributes for resisting protein adsorption from complex biological media like blood plasma. For instance, polymer coatings such as PHEAM and PFEAM demonstrated contact angles below 10° and ~30°, respectively, and were shown to reduce fouling by more than 90%. This superior performance is attributed to the formation of hydrated, brush-like polymer layers that act as physical and entropic barriers against nonspecific biointeractions.[88] Interestingly polymer brushes of poly(HPMA) show only moderate hydrophilicity, but yet are considered as the most effective in suppressing fouling from various biological media.[119, 120] Contact angle goniometry can be used not only as a predictor of hydrophilicity and antifouling behavior but also as a method of probing surface adaptation. Block copolymer brushes, consisting of surface-tethered polymer chains with chemically distinct blocks, exhibit adaptive behavior in response to environmental stimuli such as solvent type or temperature. This adaptability arises from solvent-selective swelling, chain reorientation, and compositional restructuring at interfaces, often resulting in tunable surface properties like wettability. Surface-grafted diblock copolymer brushes composed of a hydrophilic PHEMA bottom block and a hydrophobic PS or PEtHexMA top block exhibit reversible switching between hydrophobic and hydrophilic states.[111] Exposure to warm water induces swelling and migration of the hydrophilic block to the surface, decreasing the receding contact angle, while toluene treatment and annealing restore the hydrophobic character. The adaptive response is highly dependent on the thickness of the top block: only layers thinner than ~20–30 nm allows water-induced restructuring. Advancing contact angles consistently reflect the top layer chemistry, whereas receding angles reveal deeper structural rearrangements. VSFG spectroscopic and AFM topographic analyses confirm that both surface chemistry and molecular-scale roughness govern this behavior, highlighting the role of nanoscale architecture in the dynamic wetting properties of block copolymer brushes.[111]

The role of hydration/solvation and the influence of salts, including potential Hofmeister effects, are probed via *in situ* SE. High swelling ratios which are usually observed for various hydrophilic

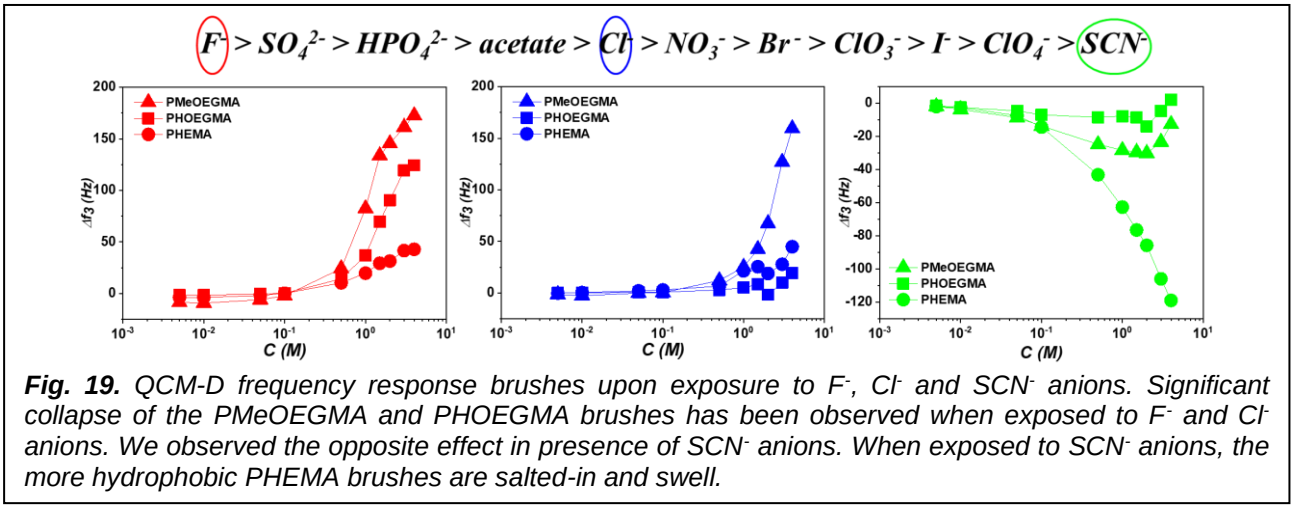

Fig. 19. *QCM-D frequency response brushes upon exposure to F^-, Cl^- and SCN^- anions. Significant collapse of the PMeOEGMA and PHOEGMA brushes has been observed when exposed to F^- and Cl^- anions. We observed the opposite effect in presence of SCN^- anions. When exposed to SCN^- anions, the more hydrophobic PHEMA brushes are salted-in and swell.*

acrylate and acrylamide polymer brushes reaching values of 5.5 indicate extensive water uptake, with $[H_2O]/[M]$ ratios reaching up to 30 for PHEAM. Interestingly, PFEAM, despite containing a fluorinated CH_2F side chain, displays a high $[H_2O]/[M]$ ratio of 20 and an *SR* of 4.3, attributable to the hydrogen-bond acceptor nature of fluorine in the $–CH_2F$ moiety. This supports its ability to form a structured hydration shell that contributes to its antifouling behavior. The adaptive behavior of the polymer brush chains and their conformational changes when exposed to various external stimuli can be monitored using parallel measurement of SE and quartz crystal microbalance with dissipation monitoring (QCM-D) (***Fig. 19***). The conformation of grafted polymer chains at the solid-liquid interface is strongly dependent on the type and concentration of salts in the surrounding liquid phase. The ion-specific interaction of PHEMA, PHOEGMA and PMeOEGMA brushes with F^-, Cl^- and SCN^- anions from the Hoffmeister series have been investigated. The increasing ionic strength of kosmotrope solutions of F^- ions led to strong collapse of the brushes. At the same time, the solutions of chaotropic SCN^- anions induced strong swelling of the polymer chains.

2.2.3. Comparative antifouling performance of polymer brushes synthesized by "grafting-from" approach. [*D1, D8, D27-D30, D34, D43-D47*]

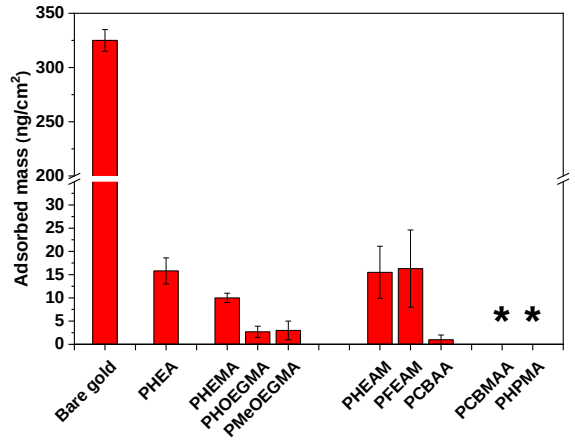

Fig. 20. *Comparison of antifouling properties of various classes of hydrophilic polymer brushes as measured by SPR. Asterix symbol (*) designates values below the detection limit of the measurement, i.e. 0.3 ng/cm²).*

Grafting-from brushes maintain dense hydration layers, even in functionalized forms, which provides exceptional resistance to protein adsorption from complex media such as undiluted blood plasma. For example, brushes based on various hydrophilic (meth)acrylate and (meth)acrylamide monomers, such as PHEMA, PHOEGMA, PMeEOGMA, PHEA, PCBAA, PHEAM, PFEAM, PHEAM, or P(HPMA-co-CBMAA) show >95% reduction in fouling from various biological media (such as blood serum, blood plasma, saliva, urine, homogenized food, etc.) relative to bare unprotected surfaces, which surpasses many "grafting-to"-based coatings.[20-23, 67, 88, 119, 121, 122] Polymer brushes based on PCBAA, PCBMA and PHPMA manage to completely suppress the fouling from blood plasma (***Fig. 20***).[15, 17, 20-23] Finally, antifouling performance contrasts sharply between brushes synthesized by grafting-from versus grafting-to. The former consistently yields lower protein adsorption from complex biological fluids, even after functionalization. For instance, PFEAM brushes resist >95% of protein fouling from undiluted plasma, rivaling hydroxy-functionalized counterparts despite lacking classical hydrophilic groups.[88] Remarkably, in spite of the lack of the hydroxy group, PFEAM displayed a hydrophilic character. Besides the presence of the amide group, the hydrophilicity can be attributed to the hydrogen-bond accepting ability of the $R–CH_2F$ group, which is, in general, higher compared to the $R–CHF_2$ and $R–CF_3$ moieties.[123, 124] As mentioned in the introduction, at least a moderate degree of surface hydrophilicity is usually considered a requirement for resistance to fouling from blood plasma proteins. It is intriguing that the PFEAM brush is hydrophilic even though it does not display charged, zwitterionic or hydroxy groups and it contains a F atom. It is noteworthy to mention that while PHEAM displayed higher wettability compared to the PFEAM brushes counterparts, this did not translate into a superior resistance to fouling. [125] Adequate hydrophilicity is crucial to prevent fouling initiation through hydrophobic interactions. However, as it was previously reported [126-129], simply increasing surface hydrophilicity beyond a certain point does not guarantee enhanced fouling prevention. In swollen state, similar to PHEA and PHEAM counterparts, the PFEAM chains extend as a result of the absorption of a specific quantity of water molecules trapped by the hydrogen bonding interactions with the hydrophilic functional groups of the polymer. Furthermore, this unique combination of factors imparts PFEAM film with a remarkable ability to resist protein fouling, particularly from human blood plasma, displaying an effectiveness of over 95% compared to the reference, notwithstanding the lack of hydroxy groups or a zwitterionic character. This discovery

underscores the versatility of the PFEAM coating, making it suitable not only for ^{19}F MRI diagnostic applications but also for a wide range of uses requiring antifouling materials. Similarly, copolymer brushes of HPMA and CBMAA demonstrate negligible fouling from biological media and retain antifouling properties even after high-density ligand immobilization, overcoming the fouling issues seen with brushes modified post-synthesis via grafting-to strategies (***Fig. 20***).[10, 20-23, 102] In conclusion, the "grafting-from" technique enables the fabrication of advanced polymer brush architectures with controlled vertical composition (further elaborated in section 2.3.1), high hydration, and excellent non-fouling behavior. These characteristics make them indispensable for high-performance surfaces in biosensing and blood-contacting applications.

2.2.4. Functional implications and applications of polymer brushes synthesized via the "grafting-from" avenue.

Polymer brushes synthesized via the *"*grafting-from*"* approach offer high grafting density, tunable thickness, and precise compositional control, resulting in surfaces with exceptional functional performance. These brushes form dense, hydrated layers that provide robust resistance to protein adsorption from complex biological media, making them ideal for antifouling applications. Their responsiveness to environmental stimuli, such as solvent, pH, or temperature, enables dynamic tuning of surface properties. Additionally, the preserved chain-end functionalities allow for post-polymerization modifications, facilitating the incorporation of bioactive or clickable groups without compromising antifouling performance. These features support a wide range of applications, including non-fouling coatings for biomedical devices, biosensing platforms with selective biorecognition, tissue engineering scaffolds with spatially controlled cell interactions, and smart surfaces for controlled adhesion or release, controlled adaptation or of sustained unidirectional motion (durotaxis) of droplets without external energy supply when placed on a polymer brush substrate with stiffness gradient in a certain direction. Moreover, the ability to create vertically and laterally structured architectures extends their use to micro- and nano-scale patterning, with demonstrated utility in diagnostics, marine antifouling, and responsive coating technologies. The developed toolbox can serve as a starting point towards the envisaged autonomous surfaces of various lateral, hierarchical and time-line encodings.

2.3 Surface analysis -From macroscopic analysis to surface nanoscopy. [*D2, D3, D11, D24, D48*]

My research group has focused on the comprehensive understanding of physical, chemical and biological phenomena taking place at biointerfaces. Within our existence we focus not only on synthesis and adopting various state-of-the-art analytical techniques for the characterization of surfaces and biointerfaces, but we target profound understanding, considered computational and theoretical approaches for spectral analysis and further developed methods to obtain reliable data analysis. In all cases we address surface design and analysis on the basis of a synergistic combination of far-field macro-/micro–scopic and near-field nanoscopic analytical techniques. Our joint projects implemented a plethora of techniques and methods (the results of which are the basis of the analysis of the previous (sub–)chapters), such as AFM identification of surface confluent particles, multiple-sample and multiple-environment variable-angle spectroscopic ellipsometry (VASE), design of *in situ* probes/cuvette VASE, spectroscopic Brewster angle microscopy for the model free determination of optical dispersion functions of refractive indexes of solutions, *in situ* GAATR-FTIR spectroscopic analysis in water, simulation of X-ray photoelectron spectra and vibrational IR spectra using quantum mechanics, multivariate analysis of FTIR spectra techniques (principal component analysis, partial least squares regression analysis and Fourier self-deconvolution)[130], electro-kinetics (streaming current) measurements analyzed by applying the theory for the electrohydrodynamics of diffuse soft interfaces[10], etc.). Within this section, I will put the accent on the most important and unique developments of techniques and results. Specifically, we have utilized XPS depth profiling, QCM-D combined with *in situ* VASE, and nanoscale Fourier-transform infrared spectroscopy (nanoFTIR) to probe the chemical, structural, mechanical, and conformational properties of end-tethered polymer chains. These approaches have enabled a deeper understanding of the polymer brush architecture and its response to environmental conditions, which is essential for designing advanced surfaces.

2.3.1. Macroscopic characterization via XPS analysis and depth profiling. [*D4, D21, D35, D49-D61*]

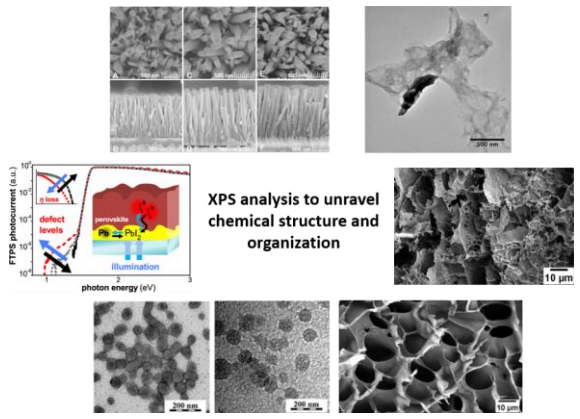

Fig. 21. *XPS analysis as a method to unravel the chemical structure and organization of various materials.*

XPS played a critical role in the characterization of a diverse range of advanced materials examined across these studies, including carbon-based aerogels, conductive polymers, hydrogels, polymer brushes, and nanoparticle systems (***Fig. 21***). In thermally treated polypyrrole-gelatin aerogels, XPS was used to monitor the evolution of carbon and nitrogen functionalities with increasing carbonization temperature, revealing enhanced graphitization through increasing sp^2 content. In graphene oxide-based nanocomposites and conductive PANI–CNF–PVP cryogels, XPS confirmed the incorporation of carbon nanofilers, induced chemical changes, changes in the sp^2/sp^3 carbon ratio and nitrogen bonding states.[131-134] For several polyelectrolyte nanoparticles, especially those formed from HPMA-based block copolymers with heparin, XPS analysis provided essential surface composition data, distinguishing between heparin-rich and polymer-rich surfaces depending on zeta potential.[135] This surface sensitivity also enabled quantification of peptide immobilization (e.g., RGDS) on functional hydrogels, where we revealed the formation of amide bonds and a significant increase in nitrogen content, confirming successful peptide conjugation.[136] In materials functionalized for achieving antifouling properties purposes, XPS confirmed covalent anchoring of the brushes via sulfur-gold bonding of polymers and initiator molecules, providing chemical insights supporting the observed resistance to protein fouling.[9, 103] Similarly, in dendrimer-modified magnetic microspheres, XPS revealed increasing surface nitrogen and oxygen content, validating the peptide dendrimer attachment through emerging amide groups.[137] Across all systems, high-resolution spectra of C 1s, N 1s, and S 2p regions enabled deconvolution of overlapping functional groups, such as amides, esters, and thiols/sulfates, facilitating precise interpretation of chemical modifications. The adopted procedures were shown indispensable in the characterization of the surface properties of inorganic materials such as ZnO based nanomaterials, ZnO nanocolums grown from the surface and study the defects in perovskite based solar cells based on lead halides.[138-142] The provided XPS analysis was found essential for probing surface chemistry of the most outed interfacial layer, confirming molecular functionalization, and validating structural models.

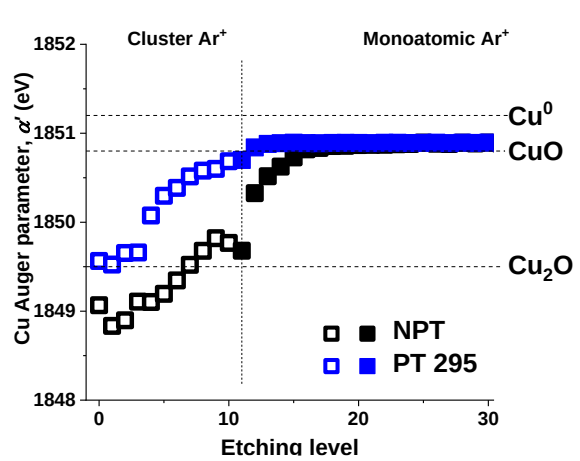

Fig. 22. *Analysis of XPS depth profiling data obtained from copper surfaces exhibiting complex Cu 2p spectral structures. Further details of developed method employing analysis of Cu LMM Auger spectra, Cu 2p and Wagner plots can be found in D61.*

Various sputtering methods can be utilized to unravel the composition further away from the most outer surface. XPS depth profiling using Ar^+ monoatomic and cluster ions present distinct challenges, especially for organic and polymeric materials (***Fig. 22*** and ***Fig. 23***). Monoatomic Ar^+ ions, while effective for sputtering metals and inorganics, can cause significant chemical damage to polymers (breaking bonds, inducing cross-linking, and altering oxidation states) thereby distorting compositional data and blurring interfaces. In contrast, Ar^+ cluster ions (composed of a defined number or argon atoms within the cluster ranging from 1000–8000 atoms) offer gentler sputtering that better preserves chemical integrity in soft materials, making them more suitable for profiling of polymers. However, cluster ions have limited efficiency in sputtering dense or inorganic layers, and depth calibration becomes

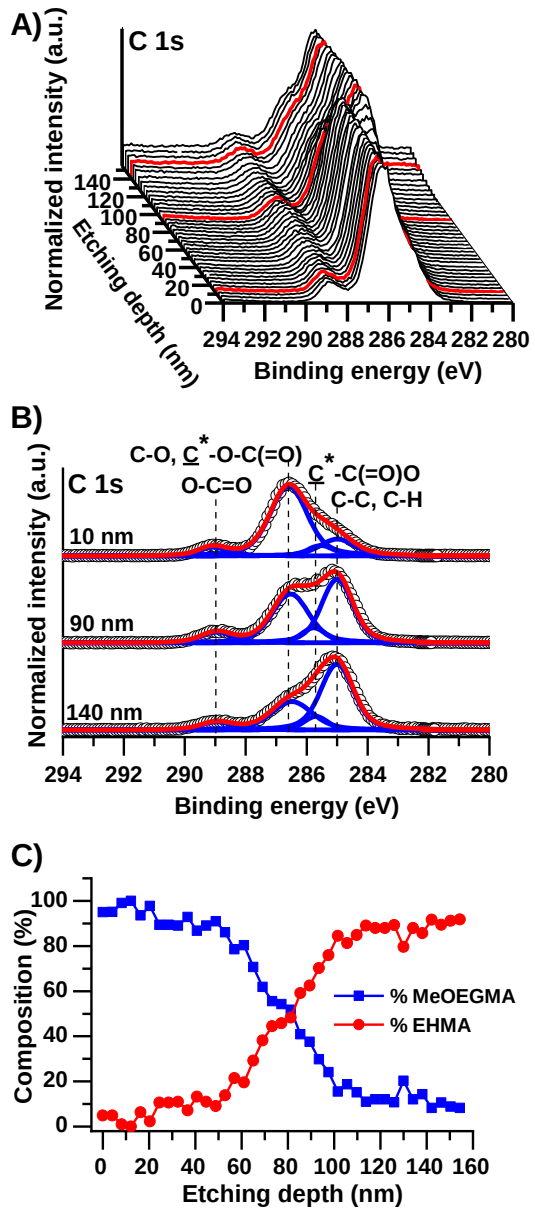

Fig. 23. *XPS depth profile of PEHMA-b-PMeOEGMA brushes. A) Evolution of C 1s XPS spectrum with etch depth. B) Deconvolution of representative C 1s XPS spectra at three etch depths. C) Approximate ratio of MeOEGMA (■) and EHMA (●) monomer units in PEHMA-b-PMeOEGMA brushes over etch depth. The total thickness of the PEHMA-b-PMeOEGMA layer was 150.4 ± 4.0 nm.*

complex due to varying sputter rates across different materials. Accurate profiling thus requires carefully balancing ion type and energy to maintain both depth resolution and chemical fidelity.

XPS depth profiling of plasma-treated copper connectors revealed a substantial reduction in surface oxides following N_2/H_2 plasma treatment, with a compositional shift from Cu^{2+}/Cu^{1+} species at the outermost surface toward metallic Cu^0 at greater depths (***Fig. 22***). This confirmed effective removal of organic and oxidized layers, correlating with enhanced wettability observed in soldering tests. However, a thin residual oxide layer remained, indicating that while plasma activation significantly improves solderability, the use of flux is still necessary to achieve full wetting.[143]

In contrast, XPS depth profiling of block copolymer brushes across multiple studies consistently demonstrated the formation of well-defined layered structures trough the employment of CP methods. The analysis of poly(t-butyl acrylate)-*b*-poly(2-hydroxyethyl acrylate) P*t*BA-b-PHEA) brushes synthesized by photo-SET-LRP showed a clear transition from an HEA-rich surface to a *t*BA-rich region at the substrate, supported by systematic shifts in C 1s peak ratios and corroborated by ToF-SIMS localization of bromine at both the surface and initiator interface, indicating living chain-end functionality.[118] Similarly, poly(2-ethylhexyl methacrylate)-b-poly(oligo(ethylene glycol) methyl ether methacrylate) PEtHexMA-b-PMeOEGMA brushes synthesized by photo-SET-LRP demonstrated a gradual depth-dependent shift in chemical composition, with quantitative mapping of C 1s signatures confirming surface enrichment originating from the PMeOEGMA and deeper localization of the PEHMA block near the substrate surface (***Fig. 23***).[67] Depth profiling of PHEMA-b-PS and PHEMA-b-PEtHexMA brushes also confirmed vertical segregation/structuring, with hydrophobic blocks dominating the air interface and PHEMA signatures increasing with etch depth.[111] These results were further validated by VSFG spectroscopy, which further revealed the presence of PS block at the air/polymer brush interface. The block copolymer brushes undergo solvent-induced rearrangements in brush surface composition as verified by the VSFG, demonstrating the dynamic nature of these stratified polymer architectures. [111]

2.3.2. Probing the viscoelastic response and molecular parameters of polymer brushes by combining QCM-D and in situ VASE. [*D3*]

The combined use of QCM-D and *in situ* VASE provides a powerful strategy to probe the viscoelastic response and extract key molecular parameters of polymer brushes, specifically PMeOEGMA (***Fig. 24***). Polymer brushes were synthesized from surface immobilized initiator

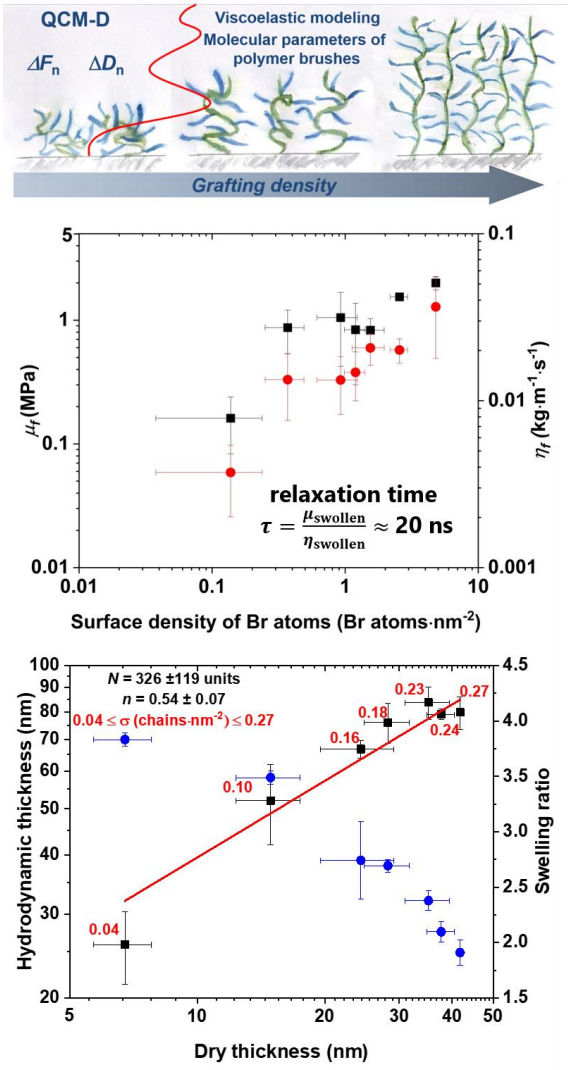

Fig. 24. *Probing the viscoelastic response and scaling behavior of poly(MeOEGMA) chains as a method of probing their surface related parameters and brush structure.*

molecules of various grafting densities via SI-ATRP. [144] QCM-D was used to monitor changes in resonance frequency (Δ*f*) and dissipation (Δ*D*) in both air and water environments, while VASE provided complementary measurements of dry and swollen layer thicknesses and refractive indices. These data were integrated using the Voigt viscoelastic model to determine hydrodynamic thickness, shear modulus (*μ*), and shear viscosity (*η*) of the swollen brushes. Notably, all brush layers, regardless of initiator density, exhibited similar characteristic relaxation times ($\tau \approx 20$ ns), indicating a uniformly stretched conformation consistent with the polymer brush regime. Hydrodynamic thickness peaked at high initiator densities (~80 nm) and declined at lower densities, suggesting reduced crowding and extension of chains.

The scaling behavior of swollen thickness versus dry thickness $h_{hydrodynamic} = 1.13^{-2n} \cdot (N \cdot a)^{1-n} \, {h_{dry}}^{n}$ was used to determine molecular characteristics, yielding a scaling exponent (*n*) of 0.54 ± 0.07, a monomer count per chain (*N*) of approximately 326 ± 119, and an estimated molar mass near 98 ± 35 kg/mol. Grafting densities *σ* spanned from 0.04 to 0.27 chains·nm^{-2}, and the reduced grafting density parameter ($\Sigma = \sigma\pi R_g^2$) ranged from 5 to 33, which confirms a highly stretched, densely packed brush conformation (***Fig. 24***). These findings demonstrate that even at varied grafting densities, PMeOEGMA brushes maintain consistent mechanical properties and hydration behavior, attributed to steric hindrance from the bulky side chains and strong perpendicular swelling. The integration of QCM-D and VASE thus enabled not only a comprehensive viscoelastic characterization but also quantitative determination of brush architecture in the hydrated state. These capabilities would be difficult to achieve with either method alone. The combined approach offers a robust framework for analyzing other polymer brush systems and paves the way for tailoring interfacial materials in biomedical and antifouling applications.

2.3.3. Nanoscopic Conformational Analysis Using sSNOM and nanoFTIR. [*D24*]

sSNOM and nanoFTIR spectroscopy were employed to achieve nanoscale characterization of ultrathin polymer brush coatings composed of poly(ethylene oxide) (PEO) grafted onto polydopamine (PDA) anchor layers (***Fig. 25***).[86] These techniques allowed for simultaneous topographical and chemical imaging with spatial resolution below 100 nm, revealing intricate structural and conformational details unresolvable by conventional methods such as AFM or far-field IR spectroscopy. For PEO brushes with molecular mass of 5 kg·mol^{-1} and 10 kg·mol^{-1}, sSNOM imaging showed uniform surface morphology and homogeneous infrared (IR) amplitude (connected to refractive index) and phase (connected to absorption coefficient) contrast at the characteristic C–O–C stretching vibration (~1113 cm^{-1}), indicating conformational uniformity and consistent brush density. In contrast, 20 kg·mol^{-1} PEO brushes exhibited a quasi-periodic nanopattern of hills and valleys with lateral spacing around 60 nm, observable in both topography and near-field IR images. The IR contrast correlated strongly with height variations, suggesting structural differences not only

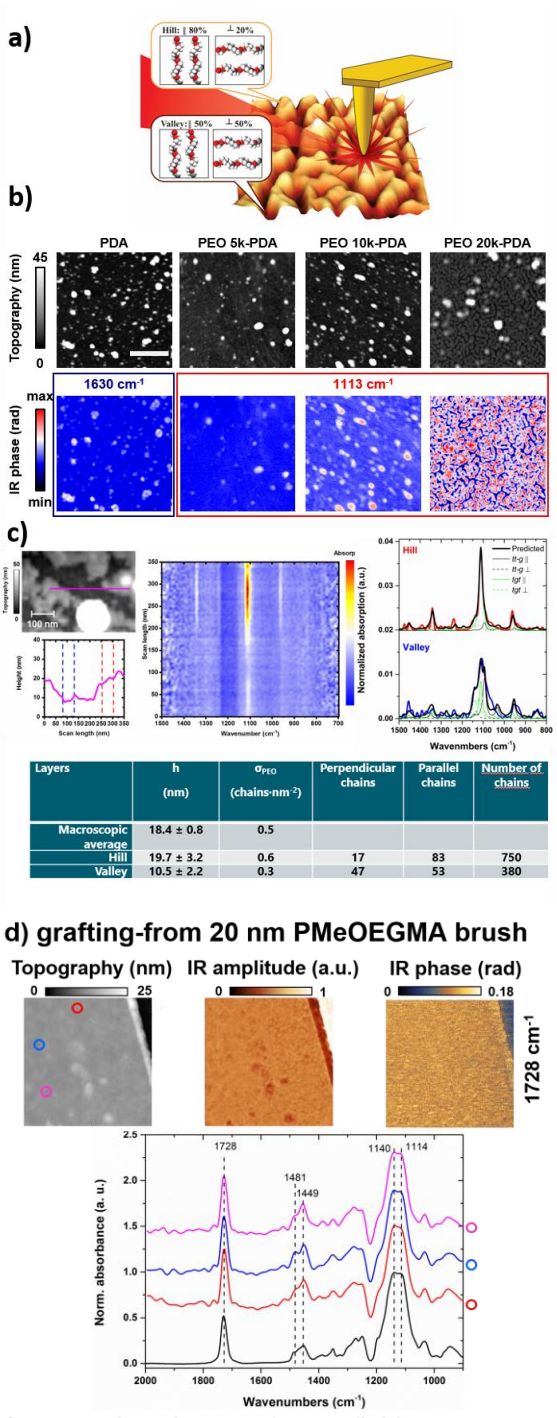

Fig. 25. *a) Scheme of near-field* sSNOM *and nano-FTIR analysis of PEO brushes "grafted-to" PDA . b)* sSNOM *analysis of PDA and PEO at different wavelengths map different vibrations of molecular species present on the brush surface. c) Unraveling the orientation of PEO chains constituting the brush layer in distinct valley and hill regions by merging nano-FTIR and DFT calculations. d) Nanoscopy performed on 20 thick PMeOEGMA brushes synthesized via the "grafting-from" method.*

in thickness but also in chain organization. NanoFTIR spectroscopy further resolved these differences, showing that hill regions exhibited stronger absorbance at 1113 cm^{-1} and at 1340 cm^{-1} (CH_2 wagging), both associated with axial chain vibrations. This indicated that polymer chains in these elevated regions were preferentially oriented perpendicularly to the surface, consistent with crystalline ordering. Conversely, valley regions showed more intense absorption at 1142 cm^{-1}, corresponding to chain segments oriented parallel to the substrate, typical of amorphous conformations. To quantify these differences, the researchers performed density functional theory (DFT) calculations on short model PEO segments (EO_8), generating vibrational spectra for distinct conformers, primarily *tgt* and *tg-g*, under both parallel and perpendicular orientations relative to the probing field. Using partial least square regression to fit the experimental nanoFTIR spectra, they determined that hill regions predominantly consisted of *tgt* conformers (more than 70%) aligned with the probing field, confirming high crystallinity and vertical orientation. In contrast, valley regions contained a broader mix of *tg-g* and *tgt* conformers with less preferential orientation, consistent with an amorphous state. The overall estimated crystallinity of the 20 $kg \cdot mol^{-1}$ brush layer was approximately 60%, with the polymer chains in the valley regions still present, resolving prior ambiguity about polymer depletion in such topographic depressions.

These findings underscore the power of sSNOM and nanoFTIR to spatially resolve chemical and structural heterogeneities in nanometer-thick polymer coatings. They not only offer insights into local polymer brush conformation and phase behavior but also reveal the interplay between grafting density, chain mobility, and crystallization. Unlike AFM, which provides only relative height and mechanical phase information, near-field IR spectroscopy adds orientation-sensitive chemical specificity, enabling the detection of conformational transitions at the nanoscale. These capabilities are especially relevant for understanding and optimizing functional polymer surfaces. The demonstrated methodology also suggests potential for future extensions, including imaging under varying environmental conditions (e.g., humidity, temperature, or liquid exposure) and adapting sSNOM for tomographic depth profiling of multilayered coatings.

2.4 Bridging the gap between “grafting-to” and “grafting-from”. [*D2, D40*]

Despite the widespread employment of polymer brushes, a systematic, quantitative comparison of “grafting-to” and “grafting-from” techniques under controlled molecular parameters has long remained unaddressed. The challenge lies in achieving a fair comparison: while the “grafting-to” method allows straightforward control of polymer molar mass prior to grafting, it suffers from low grafting densities due to steric hindrance during surface attachment. Conversely, the “grafting-from” approach enables high grafting densities through surface-initiated polymerization but complicates molar mass determination, since the polymer is synthesized directly on the substrate. The difficulty in accessing the molar mass and distribution of surface-grafted polymer generated during SI polymerizations comes from the fact that its mass is extremely low, making analysis by typical methods such as size exclusion chromatography very complicated. While some authors have assumed that the molar mass of the surface-grafted polymer is comparable with that of the polymer grown concomitantly in solution during the SI-polymerization, experimental studies have demonstrated that the polymer molar mass on the surface and the solution-born polymers may be similar or differ greatly, depending on polymerization conditions. Genzer’s and Spencer’s groups attributed this discrepancy to a phenomenon they termed “crowding” during SI-ATRP polymerization at high grafting density and/or with a high propagation rate.[145-147]

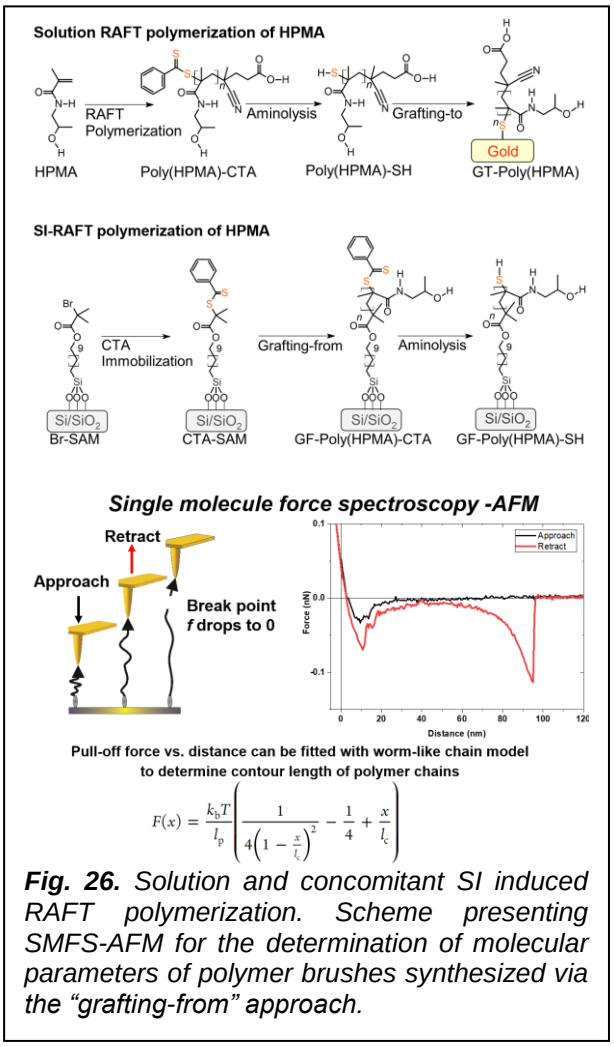

Fig. 26. *Solution and concomitant SI induced RAFT polymerization. Scheme presenting SMFS-AFM for the determination of molecular parameters of polymer brushes synthesized via the “grafting-from” approach.*

To overcome this obstacle, we developed a robust experimental strategy that enabled direct comparison between “grafting-to” and “grafting-from” methods using PHPMA brushes with precisely matched molecular characteristics (***Fig. 26***).[89, 90] Using reversible addition–fragmentation chain transfer (RAFT) polymerization, PHPMA chains were synthesized for “grafting-to”, and surface-initiated RAFT polymerization was used for “grafting-from” on SiO_2 substrates. Notably, the molar mass of surface-grafted “grafting-from” chains was determined using single-molecule force spectroscopy based on atomic force microscopy (SMFS-AFM). This technique allowed accurate quantification of the contour length and thus the molar mass of individual polymer chains tethered to the surface. Thus, we enabled a breakthrough in characterizing “grafting-from” polymer brushes without requiring polymer recovery from the surface through cleavage of the polymer chains.[89, 90] For “grafting-to” brushes, PHPMA was synthesized in solution, end-functionalized with thiol groups, and grafted onto gold substrates under both good and poor solvent conditions to modulate grafting density. Through careful tuning, “grafting-to”- PHPMA chains were matched in molar mass to those synthesized via “grafting-from” ($M_n \approx 49$ kg·mol^{-1}), verified by SEC-MALLS for “grafting-to” and SMFS-AFM for “grafting-from”. This matching of molecular characteristics eliminated a major confounding variable in previous comparisons. The results of the comparison were striking. “Grafting-to” brushes performed under good solvent conditions reached thickness of 2.0 nm, grafting density σ = 0.02 chains·nm^{-2} and distance between grafting sites D = 7.2 nm. The reduced quality of the solvent, dictating smaller R_g of polymer chains and smaller excluded volume effects led to increased thickness of 4.1 nm, σ = 0.05 chains·nm^{-2} and D = 5.0 nm. On the contrary the “grafting-from” brushes performed via SI-RAFT exhibited significantly higher thickness of 13.5 nm dry, σ = 0.18 chains·nm^{-2} and D = 2.6 nm. This translated to more compact

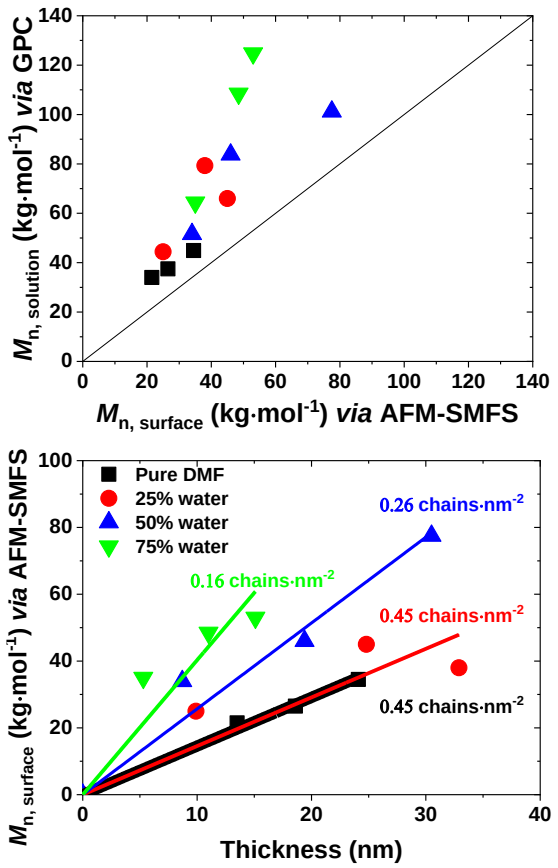

Fig. 27. *Comparison between molar mass of polymer chains formed in solution and from the surface via RAFT. Determination of σ of polymer chains synthesized via SI-RAFT.*

spacing between grafting sites and higher chain stretching in "grafting-from" layers ($D/2R_g$ = 0.18) versus "grafting-to" brushes ($D/2R_g$ = 0.34–0.49), placing the "grafting-from"-PHPMA in a more pronounced brush regime.[89] When subjected to fouling assays using human blood plasma, "grafting-from"- PHPMA brushes demonstrated an order-of-magnitude reduction in protein adsorption compared to their "grafting-to" counterparts. SPR measurements showed that "grafting-from" brushes adsorbed less than 1% of the plasma protein mass observed on bare gold, and roughly 5–10× less than even the best-performing "grafting-to" layers. These results align with theoretical models where a high-density brush presents both a hydration-based enthalpic barrier and an entropic barrier due to chain stretching, synergistically preventing protein approach and insertion into the brush layer.[89] Understandably, the achieved polymer surface parameters of grafted PHPMA via SI-RAFT seems to fail behind possible maximal density of highly overlapping polymer chains, approaching distances between polymer chain as small as the size of a monomer unit the density via the SI-RAFT. We therefore extended this comparison by investigating the solvent effects on SI-RAFT polymerization of PHPMA (***Fig. 27***). By systematically varying solvent polarity and proticity (DMF/water and 1,4-dioxane/water systems), the study demonstrated that solvent composition strongly influences both polymer growth rate and grafting density. While higher water content in solvent mixtures increased the propagation rate and molar mass of solution-grown polymers, it led to decreased grafting densities on surfaces due to mass transport limitations and swelling-induced steric hindrance. For instance, in pure dimethylformamide (DMF), the grafting density was 0.48 chains·nm^{-2}, but dropped to 0.16 chains·nm^{-2} when the water content in the solvent system was increased to 75%. These findings were verified using a solvent system composed of 1,4-dioxane/water. This discrepancy was visually validated by comparing molar mass distributions and dry film thicknesses measured by ellipsometry and SMFS. The ratio of solution-grown to surface-grown molar masses ($M_{n,\ sol}/M_{n,\ sur}$) increased at higher water content, confirming diffusion-limited surface growth under faster propagation conditions.

In summary, the combined results provide the first quantitative, head-to-head assessment of "grafting-to" and "grafting-from" PHPMA brushes with matched molecular parameters. The SMFS-AFM method for in situ molar mass determination of "grafting-from" chains resolves a longstanding analytical bottleneck and enables fair comparison with "grafting-to" layers. These findings conclusively demonstrate that the "grafting-from" approach, by inherently enabling higher grafting density and true brush formation, confers markedly superior antifouling behavior, even when polymer chemistry and chain length are held constant. Furthermore, these studies show even how to tune the grafting density of polymer brushes performed by the SI-RAFT approach. While "grafting-to" offers simplicity and ease of fabrication, "grafting-from" enables higher densities and superior antifouling, albeit requiring stringent conditions. Poor solvent grafting can partially enhance "grafting-to" density, but still falls short of "grafting-from" method's capabilities. As such, "grafting-from"-PHPMA brushes emerge as a the most promising platform for the design of next-generation antifouling materials.

Chapter 3 – Bioactive polymer-based systems as functional interfaces for biosensing and biomedical applications. [D6, D12, D14, D22, D26-D30, D36, D37, D39, D42, D47, D62]

In this part, we turn to the development and application of advanced bioactive polymer-based systems as functional interfaces tailored for biosensing and biomedical technologies. These systems are designed to selectively interact with biological components, resist non-specific interactions, and support tissue-specific responses. A central focus is placed on the implementation of anti-fouling, hierarchically structured polymer brushes bearing ECM-derived peptide motifs. These platforms are engineered to detect protein biomarkers in complex biological media with high specificity and to support regenerative processes through cell-instructive biointerfaces. Protein-repulsive surfaces that can be selectively modified with bioactive ligands offer an effective route toward controlled molecular recognition and cell adhesion.

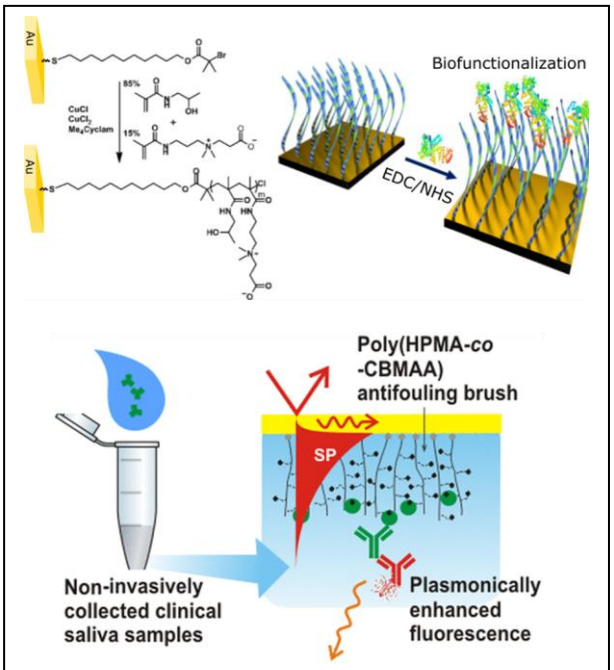

Fig. 28. *P(CBMA-ran-HPMA), offer advantages for antifouling coatings and biosensing applications.*

Among various strategies, surface-tethered polymer brushes, particularly those prepared SI-ATRP have emerged as robust antifouling coatings.[10, 13, 18, 19, 91, 102] We have shown that copolymer brushes, particularly those composed of P(CBMA-*ran*-HPMA), offer advantages for antifouling coatings and biosensing applications. Their architecture, integrating zwitterionic (CBMA) and nonionic (HPMA) monomers, enables a tunable balance between fouling resistance and biorecognition element (BRE) immobilization (***Fig. 28***). A key strength lies in their ability to resist nonspecific adsorption from biological media such as blood plasma, saliva, and food homogenates even after BRE functionalization. The immobilization of antibodies, DNA probes, and antigens onto these brushes is accomplished via carbodiimide coupling chemistry, specifically using *N*-ethyl-*N'*-(3-dimethylaminopropyl)carbodiimide (EDC) and *N*-hydroxysuccinimide (NHS), which activates surface carboxyl groups in CBMA for covalent attachment to amine-bearing/functionalized BREs. To preserve antifouling performance post-functionalization, glycine is employed to deactivate residual NHS esters and restore charge neutrality. Brushes with ~15 mol% CBMA show optimal performance, supporting high probe loading (e.g., ~200 ng·cm^{-2} of antibody or 10^{13} DNA probes·cm^{-2}) while maintaining fouling resistance below 5 ng·cm^{-2}. These coatings outperform conventional OEG-based SAMs and homopolymer PCBMA in both sensitivity and selectivity towards the immobilization BRE.[20-23] Hierarchical brushes, combining a non-fouling lower block (e.g., PMeOEGMA and a reactive upper block (e.g., PMSI, PGMA), enable vertically-controlled functionalization (along the z-axis) while preserving bioinertness.[13, 113] These interfaces support “click” chemistry-based immobilization of cell adhesive motifs (RGD peptides), which recapitulate ECM to direct cellular behavior without allowing uncontrolled biofouling.[13, 19, 102]

The antifouling properties of PEO and MeOEGMA-based brushes have enabled the development of biosensing surfaces capable of detecting protein biomarkers in complex biological fluids such as blood plasma. By incorporating reactive azide or alkyne groups on the outermost layer of the polymer brushes, biomolecular recognition elements (e.g., antibodies or peptide ligands) can be covalently attached via bioorthogonal CuAAC reactions, preserving surface integrity and reducing background noise from nonspecific adsorption.[10, 19] For instance, azide-functionalized diblock copolymer brushes showed negligible fouling from undiluted fetal bovine serum and various growth media while maintaining ligand accessibility for selective binding of target analytes. A facile strategy for the creation of bioactive surfaces resides on the end-group biofunctionalization of brushes via an ultra-fast Diels-Alder “click” reaction.[128] SI-ATRP is employed to grow antifouling polymers preserving

the chain-end groups. This Br-group is then further converted to a reactive cyclopentadienyl moiety and exploited for the immobilization of biomolecules bearing maleimide groups on the topmost layer of the brush. The minimal chemical modification of the antifouling polymer brush accounts for the full preservation of the fouling resistance of the surface even after biofunctionalization. These avenues are crucial in biosensor applications, where a high SNR and long-term stability in protein-rich environments are mandatory.

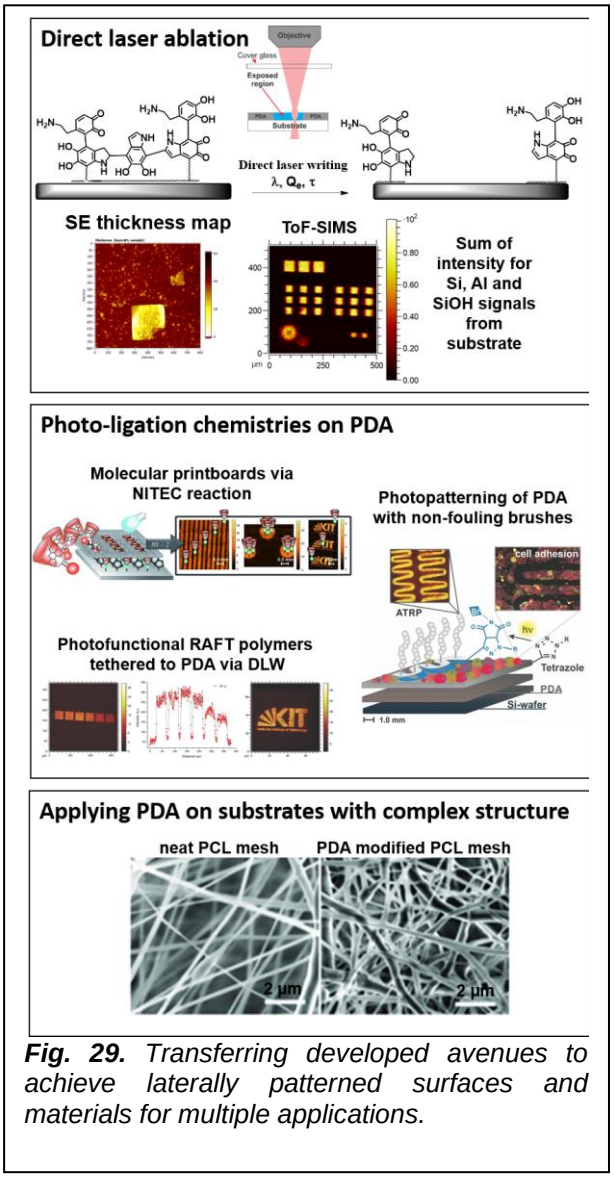

Fig. 29. *Transferring developed avenues to achieve laterally patterned surfaces and materials for multiple applications.*

To extend the biofunctionality of antifouling coatings beyond biosensing, we engineered implantable surfaces to support tissue regeneration. Direct laser writing (DLW) was employed to achieve ablating of the PDA and PDA-polymer brush surfaces to achieve patterned surface wells in which proteins could be deposited (***Fig. 29***). By lateral patterning of initiator polymer brushes we have introduced beta-cyclodextrin (CD) based supramolecular devices, presenting a novel tool to fabricate multifunctional biointerfaces. Precision photolithography of a modified beta-CD was established on a light sensitive tetrazole surface immobilized on a PDA anchor layer via various shadow masks, as well as via DLW, in order to achieve a printboard design. Interfacial molecular recognition provided by light generated cavitate domains was demonstrated via spatially resolved encoding, erasing, and recoding of distinct supramolecular guest patterns (***Fig. 29***). Thus, the light directed shaping of receptor monolayers introduces a powerful path to control supramolecular assemblies on various surfaces.[115] Similarly, PDA surface confluent layers were patterned with PMeOEGMA brushes utilizing a nitrile imine-mediated tetrazole-ene cycloaddition (NITEC)-based phototriggered surface encoding protocol. The antifouling brushes were photopatterned on PDA surfaces, leading cells to form confluent layers in the non-irradiated sections, while no adhesion occurred on the brushes. The presented strategy paves the way for tailor-made laterally encoded cell interfaces based on the adsorption of ECM-proteins from biological media and that on woven mashes (***Fig. 29***).[114, 117]

Another strategy of implantable surfaces can be achieved through covalent tethering of ECM-derived peptide motifs such as RGD, Col (collagen-derived fibronectin-binding sequences), or their combinations onto PEO brushes.[10, 13, 18, 19, 91, 102] The combination of RGD and Col ligands further enhanced focal adhesion formation, as evidenced by increased expression of integrin-associated proteins (e.g., talin, vinculin) and improved adhesion under dynamic conditions (e.g., shear stress), demonstrating promise for vascular graft coatings and endothelialization strategies.[18, 102] Surface modification was successfully translated to woven polyethylene terephthalate (PET) vascular grafts (***Fig. 30***). By leveraging aminolysis and acylation reactions, ATRP initiators were immobilized onto PET surfaces, allowing direct “grafting-from” polymerization of PMeOEGMA-*b*-PGMA brushes.[13] The surface-immobilized hierarchical brushes were functionalized with RGD peptides in a wide range of surface density of $1.1 – 4.6 \times 10^3$ nmol·cm^{-2}, confirmed via radio-assay and ^{125}I-radiolabeled RGD-peptide, XPS and GAATR-FTIR.

In the case of peptide-modified PEO brushes, particularly those functionalized with RGD adhesion motifs, electrokinetic analysis reveals that binding bioactive peptides onto the distal ends of PEO chains introduces distinct interfacial charging effects without significantly compromising the nonfouling character of the brush. Streaming current measurements show a consistent shift in the point of zero streaming current to lower pH values (from ~4.9 to ~4.1) as the surface density of RGD peptides increases, indicating enhanced negative interfacial charge. This effect is attributed not only to the intrinsic ionizable groups within the peptides but also to conformational changes upon immobilization and preferential adsorption of OH^- over H_3O^+ at the peptide-functionalized interface.[10] Despite these changes in surface electrostatics, the brushes maintain low levels of protein adsorption from fetal bovine serum, with only minor fouling observed at high RGD densities primarily from positively charged proteins such as lysozyme. These findings highlight that peptide-functionalized PEO brushes can incorporate bioactivity while preserving electrostatic screening and antifouling properties. The coatings maintained antifouling characteristics while supporting the formation of dense, confluent layers of HUVECs (human umbilical vein endothelial cells). These cells colonized the modified PET surfaces both internally and externally, demonstrating efficient mimetics of natural ECM cues and long-term adhesion stability (***Fig. 30***).[13] These functional interfaces facilitate regenerative cellular responses crucial for implant integration and long-term patency in vascular applications. The hierarchical brush architecture allows for dual-functionality: shielding the material from non-specific interactions while exposing bioactive ligands to guide cell attachment.

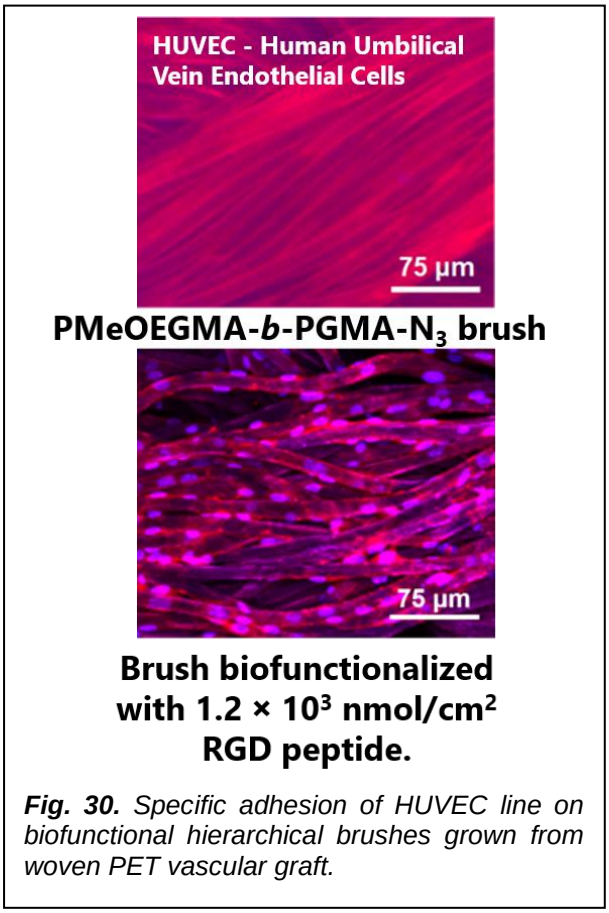

Fig. 30. *Specific adhesion of HUVEC line on biofunctional hierarchical brushes grown from woven PET vascular graft.*

The spatial presentation and surface density of ECM-derived ligands, such as RGD peptides, critically influence integrin clustering, focal adhesion formation, and downstream signaling. Studies demonstrated that low ligand densities can induce cell polarization and migration, whereas higher densities promote spreading, proliferation, and focal adhesion maturation. Fibroblasts respond differently to RGD spacing at the nanoscale, with maximum focal adhesion assembly occurring at ligand spacings of approximately 58 nm. This spatial dependency highlights the need for precise control over cue density when designing implantable biomaterials.[24, 33, 35]

sSNOM, nanoFTIR and AFM-IR have been recently used to probe the properties of biomaterials and managed to investigate the conformation of peptides, polypeptides, and proteins with a nanometer resolution. These methods provide vibrational fingerprints—particularly amide I (~1650–1670 cm^{-1}) and amide II (~1510–1560 cm^{-1}) bands—that are highly sensitive to protein secondary structure and molecular orientation.[148, 149] sSNOM analysis provided detailed imaging of nanoscale structures such as collagen *D*-banding and fibril kinking in overloaded tendons. NanoFTIR enabled chemical mapping of protein assemblies and detection of conformational changes such as α-helix to β-sheet transitions during amyloid aggregation.[76, 150, 151] Polarization-sensitive AFM-IR and nanoFTIR measurements further allow discrimination between in-plane and out-of-plane dipole orientations, providing direct insight into structural anisotropy in peptides and fibrillar proteins.[82, 152] Recently, nanoFTIR was used to probe living bacterial and cancer cells in aqueous environments, nanoscopically observing and spectroscopically characterizing living cells in their native environment. This breakthrough extends nanoFTIR into live-cell biology, opening possibilities for observing dynamic biochemical processes at the nanoscale.

We collected nanoFTIR spectra from a peptide-functionalized surface revealing orientation-sensitive vibrational features that reflect peptide conformation. The red spectrum measured at higher surface coverage shows strong amide I (~1670 cm^{-1}) and amide II (~1540 cm^{-1}) bands, characteristic of a moderately disordered or aggregated peptide layer (***Fig. 31***). In contrast, the blue spectrum recorded at lower peptide density exhibits a distinct and enhanced band at ~1590 cm^{-1}. This band is primarily attributed to the guanidinium group of arginine, which undergoes C–N stretching and NH_2 bending vibrations in this region. Its enhancement under *p*-polarized nanoFTIR suggests a geometry in which arginine side chains are oriented vertically with respect to the substrate, aligning their dipole moments with the surface-normal electric field. Importantly, tyrosine residues may also contribute to this band via aromatic ring C=C stretches (notably the *v*8b mode), which fall in a similar range. If tyrosine side chains are solvent-exposed or tilted with respect to the surface, their contribution to the ~1590 cm^{-1} intensity becomes more likely. In practice, both arginine and tyrosine side chains may contribute, especially under low-density conditions, where side chains experience greater conformational freedom and are more likely to adopt z-oriented geometries. This supports the hypothesis that the observed enhancement in the nanoFTIR spectrum could stem from the combined effect of vertically oriented arginine and tyrosine side chains. This is especially pronounced at low surface density, where conformational freedom of chain and peptides is greater. The sSNOM analysis further maps the surface density of the TYRAY peptides along the polymer brush surfaces, with distinct regions along the surface for the amide I, amide II and the vibration at ~1590 cm^{-1} (***Fig. 31***). Interestingly, we observed reversed pattern in amide I and the vibration at ~1590 cm^{-1} at high density of the TYRAY moiety over the surface. Interestingly while we observed rather uniform distribution of amide I and amide II vibrations at low peptide densities, a clear pattern of the vibration at ~1590 cm^{-1} was observed, most probably connected with adopted more z-oriented geometries of the guanidine moiety of arginine and the aromatic ring of tyrosine. The results point to the possibility of employing near-field spectroscopies for the detailed spectroscopic characterization of biointerfaces. Our future efforts will focus on developing methods for the *in-situ* characterization of interfaces in presence of surface adherent cells. The modularity, stability, and biocompatibility of antifouling polymer brushes bearing ECM-mimetic peptides make them ideal candidates for clinical translation. Applications extend beyond biosensors and vascular grafts to include coatings for stents, wound dressings, neural interfaces, etc. Scalability of surface functionalization and long-term *in vivo* performance remain important focus areas.

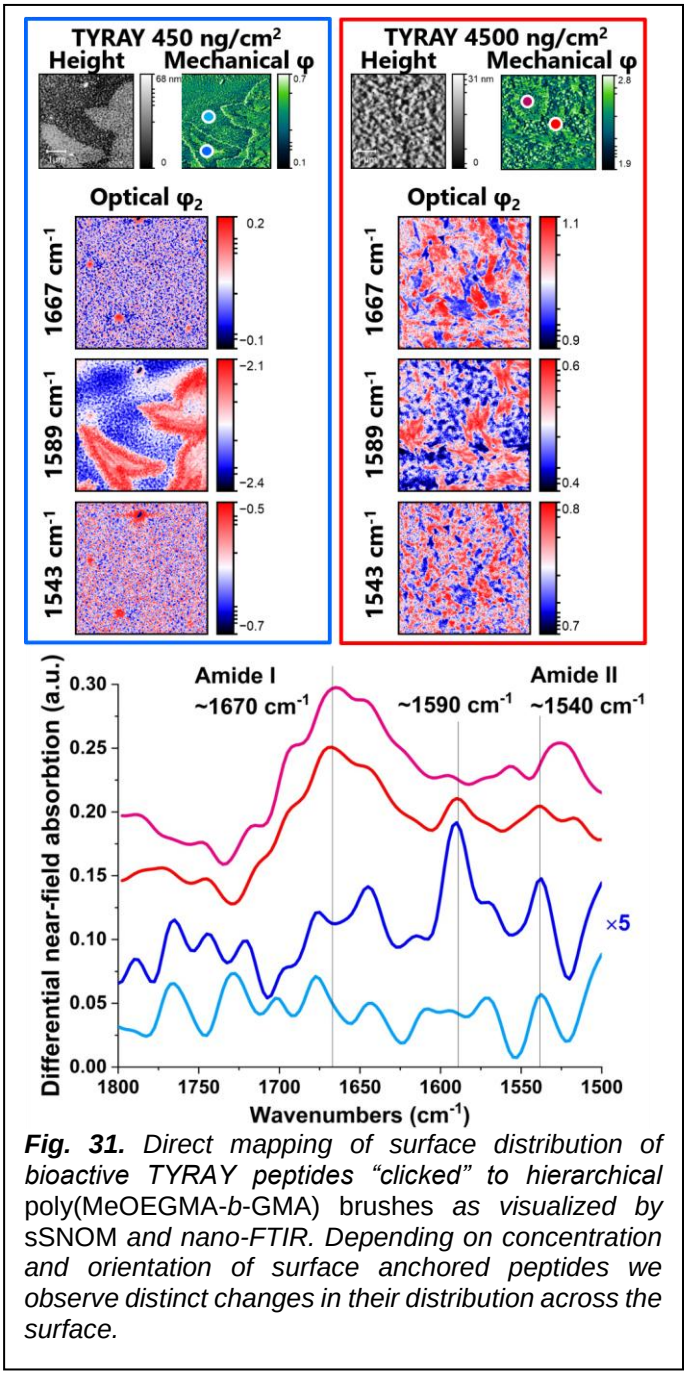

Fig. 31. *Direct mapping of surface distribution of bioactive TYRAY peptides "clicked" to hierarchical* poly(MeOEGMA-*b*-GMA) brushes *as visualized by* sSNOM *and nano-FTIR. Depending on concentration and orientation of surface anchored peptides we observe distinct changes in their distribution across the surface.*

Chapter 4 – Conclusions and challenges ahead

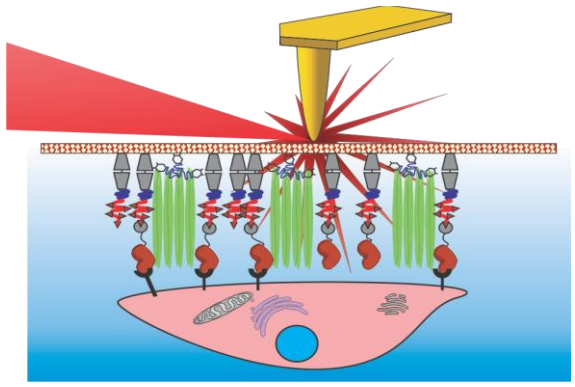

Fig. 32. *Towards in situ tip-induced near-field real-time infrared nano-spectroscopy for characterization of biointerfaces and chemical characterization of self-regulatory events at autonomous surfaces.*

In this concluding chapter, we look toward the horizon that extends from the body of work presented in this thesis. While the scientific community has made considerable strides in minimizing biofouling the current paradigm has largely revolved around reactive or preventative strategies aimed at fouling resistance. In tissue engineering and biomedical device development, this has led to surfaces that passively resist biological adhesion or require constant external intervention to maintain their functionality. However, we propose a shift toward a more dynamic, biologically integrated surfaces do not simply resist change but actively participate in it. Drawing inspiration from nature, we propose the development of *autonomous surfaces*, materials that interact with their biological environment in a fundamentally different way. In natural systems, cells are far from passive entities. They continuously sense, respond to, and remodel their surroundings based on biochemical cues, mechanical stress, and cellular communication. We foresee that future biomaterials should not only support such cellular behavior but also learn from and respond to it, establishing a bidirectional communication between the material and its cellular partners. The autonomous surfaces we envision can be achieved through herein presented macromolecular chemistry avenues and physicochemical approaches which we further develop through *in situ* nanoscale characterization (***Fig. 32***). The autonomous surfaces will be inherently capable of delivering specific molecular and mechanical signals to adherent cells. However, their function will not stop at merely transmitting signals. These surfaces will be designed to interpret cellular responses, thereby adjusting their own biochemical and physical properties. We envisage surfaces that sense the onset of inflammation and respond by releasing anti-inflammatory agents, or neural interfaces that modulate their surface topography in response to neuronal activity, enhancing integration and minimizing foreign body reactions. Importantly, the implementation of these autonomous surfaces could enhance the performance and longevity of medical devices.

Publications serving as the basis for the dissertation

(*Corresponding author, Citations according Web of Science on date 10.09.2025)

[***D1***] D.F. Dorado Daza, A. de los Santos Pereira, O. Kopilec, R. Sivkova, J. Svoboda, O. Sedlacek, **O. Pop-Georgievski***, “Grafting-from” synthesis of fluorinated acrylamide polymer brushes: From controlled polymerization to outstanding antifouling properties, Polymer 323 (2025) 128175, IF: 4.5, 1 citation.

[***D2***] Y.M. Wang, A. Kalosi, Y. Halahovets, I. Romanenko, J. Slaby, J. Homola, J. Svoboda, A. de los Santos Pereira, **O. Pop-Georgievski***, Grafting density and antifouling properties of poly[N-(2-hydroxypropyl) methacrylamide] brushes prepared by "grafting to" and "grafting from", Polymer Chemistry 13(25) (2022) 3815-3826, IF: 4.6, 35 citations.

[***D3***] I. Romanenko, R. Sivkova, J. Svoboda, T. Riedel, A. de los Santos Pereira, **O. Pop-Georgievski***, Probing the brush structure of end-tethered poly(oligo(ethylene glycol) methyl ether methacrylate) chains, Polymer 332 (2025) 128569, IF: 4.5, no citations.

[***D4***] B. Leibauer, **O. Pop-Georgievski**, M.D. Sosa, Y. Dong, W. Tremel, H.J. Butt, W. Steffen, How Surface and Substrate Chemistry Affect Slide Electrification, Journal of American Chemical Society 146(14) (2024) 10073-10083, IF: 15.6, 7 citations.

[***D5***] **O. Pop-Georgievski***, D. Kubies, J. Zemek, N. Neykova, R. Demianchuk, E.M. Chanova, M. Slouf, M. Houska, F. Rypacek, Self-assembled anchor layers/polysaccharide coatings on titanium surfaces: a study of functionalization and stability, Beilstein Journal of Nanotechnology 6 (2015) 617-31, IF: 2.8, 41 citations.

[***D6***] C. Rodriguez-Emmenegger, C.M. Preuss, B. Yameen, **O. Pop-Georgievski**, M. Bachmann, J.O. Mueller, M. Bruns, A.S. Goldmann, M. Bastmeyer, C. Barner-Kowollik, Controlled cell adhesion on poly(dopamine) interfaces photopatterned with non-fouling brushes, Advanced Materials 25(42) (2013) 6123-6127, IF: 15.4, 183 citations.
[***D7***] B. Yameen, C. Rodriguez-Emmenegger, C.M. Preuss, **O. Pop-Georgievski**, E. Verveniotis, V. Trouillet, B. Rezek, C. Barner-Kowollik, A facile avenue to conductive polymer brushes via cyclopentadiene-maleimide Diels-Alder ligation, Chemical Commununications 49(77) (2013) 8623-5, IF: 6.7, 32 citations.
[***D8***] **O. Pop-Georgievski**, C. Rodriguez-Emmenegger, A.D. Pereira, V. Proks, E. Brynda, F. Rypacek, Biomimetic non-fouling surfaces: extending the concepts, Journal of Materials Chemistry B 1(22) (2013) 2859-2867, IF: 4.5, 78 citations.
[***D9***] V. Proks, J. Brus, **O. Pop-Georgievski**, E. Vecernikova, W. Wisniewski, J. Kotek, M. Urbanova, F. Rypacek, Thermal-Induced Transformation of Polydopamine Structures: An Efficient Route for the Stabilization of the Polydopamine Surfaces, Macromolecular Chemistry and Physics 214(4) (2013) 499-507, IF: 2.5, 55 citations.
[***D10***] **O. Pop-Georgievski**, N. Neykova, V. Proks, J. Houdkova, E. Ukraintsev, J. Zemek, A. Kromka, F. Rypacek, Polydopamine-modified nanocrystalline diamond thin films as a platform for bio-sensing applications, Thin Solid Films 543 (2013) 180-186, IF: 1.9, 36 citations.
[***D11***] **O. Pop-Georgievski**, D. Verreault, M.O. Diesner, V. Proks, S. Heissler, F. Rypacek, P. Koelsch, Nonfouling poly(ethylene oxide) layers end-tethered to polydopamine, Langmuir 28(40) (2012) 14273-14283, IF: 4.2, 85 citations.
[***D12***] V. Proks, J. Jaros, **O. Pop-Georgievski**, J. Kucka, S. Popelka, P. Dvorak, A. Hampl, F. Rypacek, "Click & seed" approach to the biomimetic modification of material surfaces, Macromolecular Bioscience 12(9) (2012) 1232-42, IF: 3.7, 40 citations.
[***D13***] **O. Pop-Georgievski***, S. Popelka, M. Houska, D. Chvostova, V. Proks, F. Rypacek, Poly(ethylene oxide) layers grafted to dopamine-melanin anchoring layer: stability and resistance to protein adsorption, Biomacromolecules 12(9) (2011) 3232-42, IF: 5.5, 97 citations.
[***D14***] **O. Pop-Georgievski***, R. Zimmermann, I. Kotelnikov, V. Proks, D. Romeis, J. Kucka, A. Caspari, F. Rypacek, C. Werner, Impact of Bioactive Peptide Motifs on Molecular Structure, Charging, and Nonfouling Properties of Poly(ethylene oxide) Brushes, Langmuir 34(21) (2018) 6010-6020, IF: 3.7, 12 citations.
[***D15***] J. Svoboda, M. Král, M. Dendisová, P. Matějka, **O. Pop-Georgievski***, Unraveling the influence of substrate on the growth rate, morphology and covalent structure of surface adherent polydopamine films, Colloids and Surfaces B: Biointerfaces 205 (2021) 111897, IF: 5.4, 29 citations.
[***D16***] M. Kral, M. Dendisova, P. Matejka, J. Svoboda, **O. Pop-Georgievski**, Infrared imaging of surface confluent polydopamine (PDA) films at the nanoscale, Colloids and Surfaces: B Biointerfaces 221 (2023) 112954, IF: 5.4, 8 citations.
[***D17***] M. Kral, M. Dendisova, J. Svoboda, A. Cernescu, M. Svecova, C.M. Johnson, **O. Pop-Georgievski**, P. Matejka, Nano-FTIR spectroscopy of surface confluent polydopamine films - What is the role of deposition time and substrate material?, Colloids and Surfaces B Biointerfaces 235 (2024) 113769, IF: 5.6, 7 citations.
[***D18***] J. Svoboda, O. Sedlacek, T. Riedel, M. Hruby, **O. Pop-Georgievski***, Poly(2-oxazoline)s One-Pot Polymerization and Surface Coating: From Synthesis to Antifouling Properties Out-Performing Poly(ethylene oxide), Biomacromolecules 20(9) (2019) 3453-3463, IF: 5.4, 42 citations.
[***D19***] D. Jirak, J. Svoboda, M. Filipova, **O. Pop-Georgievski**, O. Sedlacek, Antifouling fluoropolymer-coated nanomaterials for (19)F MRI, Chememical Communications 57(38) (2021) 4718-4721, IF: 5.4, 29 citations.
[***D20***] T.A. Tunca Arın, D. Havlíček, D.F. Dorado Daza, N. Jirát-Ziółkowska, **O. Pop-Georgievski**, D. Jirák, O. Sedlacek, Water-soluble fluorinated copolymers as highly sensitive 19F MRI tracers: From structure optimization to multimodal tumor imaging, Materials Today Bio 31 (2025) 101462, IF: 10.2, 2 citations.
[***D21***] J. Svoboda, N. Lusiani, R. Sivkova, **O. Pop-Georgievski***, O. Sedlacek, Antifouling Properties of Poly(2-Oxazoline)s and Poly(2-Oxazine)s: Direct Comparison of Polymer-Coated Surfaces with the Same Coating Parameters, Macromolecular Rapid Communications 44(17) (2023) e2300168, IF: 4.2, 12 citations.

[***D22***] J. Musilkova, I. Kotelnikov, K. Novotna, **O. Pop-Georgievski***, F. Rypacek, L. Bacakova, V. Proks, Cell adhesion and growth enabled by biomimetic oligopeptide modification of a polydopamine-poly(ethylene oxide) protein repulsive surface, Journal of Material Science: Materials in Medicine 26(11) (2015) 253, IF: 2.3, 11 citations.
[***D23***] O. Kopilec, J. Svoboda, R. Sivkova, O. Sedlacek, **O. Pop-Georgievski***, Effect of Side Groups on the Surface Parameters and Antifouling Properties of Poly(N-Alkyl Acrylamide)-Coated Surfaces, Macromolecular Chemistry and Physics 226(14) (2025) 70001, IF: 2.7, no citations.
[***D24***] A. de los Santos Pereira, A. Cernescu, J. Svoboda, R. Sivkova, I. Romanenko, B. Bashta, F. Keilmann, **O. Pop-Georgievski***, Conformation in Ultrathin Polymer Brush Coatings Resolved by Infrared Nanoscopy, Analytical Chemistry 92(7) (2020) 4716-4720, IF: 7.0, 23 citations.
[***D25***] E. Mazl Chanova, **O. Pop-Georgievski**, M.M. Kumorek, O. Janouskova, L. Machova, D. Kubies, F. Rypacek, Polymer brushes based on PLLA-b-PEO colloids for the preparation of protein resistant PLA surfaces, Biomaterials Science 5(6) (2017) 1130-1143, IF: 5.8, 14 citations.
[***D26***] R. Sivkova, J. Taborska, A. Reparaz, A. de Los Santos Pereira, I. Kotelnikov, V. Proks, J. Kucka, J. Svoboda, T. Riedel, **O. Pop-Georgievski***, Surface Design of Antifouling Vascular Constructs Bearing Biofunctional Peptides for Tissue Regeneration Applications, International Journal of Molecular Science 21(18) (2020) 6800, IF: 5.9, 17 citations.
[***D27***] H. Lisalova, E. Brynda, M. Houska, I. Visova, K. Mrkvova, X.C. Song, E. Gedeonova, F. Surman, T. Riedel, **O. Pop-Georgievski**, J. Homola, Ultralow-Fouling Behavior of Biorecognition Coatings Based on Carboxy-Functional Brushes of Zwitterionic Homo- and Copolymers in Blood Plasma: Functionalization Matters, Analitical Chemistry 89(6) (2017) 3524-3531, IF: 6.0, 53 citations.
[***D28***] H. Vaisocherova-Lisalova, F. Surman, I. Visova, M. Vala, T. Springer, M.L. Ermini, H. Sipova, P. Sedivak, M. Houska, T. Riedel, **O. Pop-Georgievski**, E. Brynda, J. Homola, Copolymer Brush-Based Ultralow-Fouling Biorecognition Surface Platform for Food Safety, Analitycal Chemistry 88(21) (2016) 10533-10539, IF: 6.3, 50 citations.
[***D29***] T. Riedel, S. Hageneder, F. Surman, **O. Pop-Georgievski**, C. Noehammer, M. Hofner, E. Brynda, C. Rodriguez-Emmenegger, J. Dostalek, Plasmonic Hepatitis B Biosensor for the Analysis of Clinical Saliva, Analitycal Chemistry 89(5) (2017) 2972-2977, IF: 6.0, 47 citations.
[***D30***] T. Riedel, F. Surman, S. Hageneder, **O. Pop-Georgievski**, C. Noehammer, M. Hofner, E. Brynda, C. Rodriguez-Emmenegger, J. Dostalek, Hepatitis B plasmonic biosensor for the analysis of clinical serum samples, Biosensors and Bioelectronics 85 (2016) 272-279, IF: 7.8, 67 citations.
[***D31***] M. Vorobii, N.Y. Kostina, K. Rahimi, S. Grama, D. Söder, **O. Pop-Georgievski**, A. Sturcova, D. Horak, O. Grottke, S. Singh, C. Rodriguez-Emmenegger, Antifouling Microparticles To Scavenge Lipopolysaccharide from Human Blood Plasma, Biomacromolecules 20(2) (2019) 959-968, IF: 6.1, 14 citations.
[***D32***] M. Vorobii, **O. Pop-Georgievski**, A.D. Pereira, N.Y. Kostina, R. Jezorek, Z. Sedlkova, V. Percec, C. Rodriguez-Emmenegger, Grafting of functional methacrylate polymer brushes by photoinduced SET-LRP, Polymer Chemistry 7(45) (2016) 6934-6945, IF: 5.4, 34 citations.
[***D33***] J. Laun, M. Vorobii, A. de los Santos Pereira, **O. Pop-Georgievski**, V. Trouillet, A. Welle, C. Barner-Kowollik, C. Rodriguez-Emmenegger, T. Junkers, Surface Grafting via Photo-Induced Copper-Mediated Radical Polymerization at Extremely Low Catalyst Concentrations, Macromol Rapid Communications 36(18) (2015) 1681-6, IF: 4.6, 48 citations.
[***D34***] M. Vorobii, A. de los Santos Pereira, **O. Pop-Georgievski**, N.Y. Kostina, C. Rodriguez-Emmenegger, V. Percec, Synthesis of non-fouling poly[N-(2-hydroxypropyl)-methacrylamide] brushes by photoinduced SET-LRP, Polymer Chemistry 6(23) (2015) 4210-4220, IF: 5.7, 71 citations.
[***D35***] B. Leibauer, A. de los Santos Pereira, D.F. Dorado Daza, Y. Wang, A.S. Hazrah, **O. Pop-Georgievski**, H.J. Butt, R. Berger, Wetting of Surface Grafted Hydrophilic-b-Hydrophobic Block Copolymer Brushes, Advanced Functional Materials 35(24) (2025) 2419443, IF: 19.0, no citations.
[***D36***] R. Sivkova, J. Svoboda, J. Pánek, D. Appelhans, **O. Pop-Georgievski**, Polymer brushes based on N-methacryloxysuccinimide as platform for versatile post-polymerization modification, Progress in Organic Coatings 178 (2023) 107447, IF: 6.5, 5 citations.
[***D37***] D. Abt, B.V. Schmidt, **O. Pop-Georgievski**, A.S. Quick, D. Danilov, N.Y. Kostina, M. Bruns, W. Wenzel, M. Wegener, C. Rodriguez-Emmenegger, C. Barner-Kowollik, Designing Molecular

Printboards: A Photolithographic Platform for Recodable Surfaces, Chemistry- A European Journal 21(38) (2015) 13186-13190, IF: 5.7, 18 citations.
[***D38***] M. Singh, L. Poláková, A.D. Pereira, **O. Pop-Georgievski**, J. Svoboda, T. Riedel, S. Gupta, Z. Sedláková, V. Raus, R. Poreba, Well-defined poly(2-isopropenyl-2-oxazoline) brushes provide fouling resistance and versatility in surface functionalization, Polymer Chemistry 15(32) (2024) 3300-3310, IF: 3.9, 4 citations.
[***D39***] R. Poreba, A. de Los Santos Pereira, R. Pola, S. Jiang, **O. Pop-Georgievski**, Z. Sedlakova, H. Schonherr, "Clickable" and Antifouling Block Copolymer Brushes as a Versatile Platform for Peptide-Specific Cell Attachment, Macromolecular Bioscience 20(4) (2020) e1900354, IF: 5.0, 30 citations.
[***D40***] Y.M. Wang, A. Kálosi, Y. Halahovets, H. Benes, A.D. Pereira, **O. Pop-Georgievski***, Solvent effects on surface-grafted and solution-born poly[*N*-(2-hydroxypropyl)methacrylamide] during surface-initiated RAFT polymerization, Polymer Chemistry 15(20) (2024) 2070-2080, IF: 3.9, 6 citations.
[***D41***] N.Y. Kostina, S. Blanquer, **O. Pop-Georgievski**, K. Rahimi, B. Dittrich, A. Hocherl, J. Michalek, D.W. Grijpma, C. Rodriguez-Emmenegger, Zwitterionic Functionalizable Scaffolds with Gyroid Pore Architecture for Tissue Engineering, Macromolecular Bioscience 19(4) (2019) e1800403, IF: 3.4, 5 citations.
[***D42***] N.Y. Kostina, **O. Pop-Georgievski**, M. Bachmann, N. Neykova, M. Bruns, J. Michalek, M. Bastmeyer, C. Rodriguez-Emmenegger, Non-fouling biodegradable poly(*ε*-lactone) nanofibers for tissue engineering, Macromolecular Bioscience 16(1) (2016) 83-94, IF: 3.2, 22 citations.
[***D43***] A. de los Santos Pereira, S. Sheikh, C. Blaszykowski, **O. Pop-Georgievski**, K. Fedorov, M. Thompson, C. Rodriguez-Emmenegger, Antifouling polymer brushes displaying antithrombogenic surface properties, Biomacromolecules 17(3) (2016) 1179-1185, IF: 5.2, 73 citations.
[***D44***] Z. Riedelova, A. de Los Santos Pereira, J. Svoboda, **O. Pop-Georgievski**, P. Majek, K. Pecankova, F. Dycka, C. Rodriguez-Emmenegger, T. Riedel, The Relation Between Protein Adsorption and Hemocompatibility of Antifouling Polymer Brushes, Macromolecular Bioscience 22(11) (2022) e2200247, IF: 4.6, 14 citations.
[***D45***] T. Riedel, A. De Los Santos Pereira, J. Táborská, Z. Riedelová, **O. Pop-Georgievski**, P. Májek, K. Pečánková, C. Rodriguez-Emmenegger, Complement Activation Dramatically Accelerates Blood Plasma Fouling On Antifouling Poly(2-hydroxyethyl methacrylate) Brush Surfaces, Macromolecular Bioscience (2022) 2100460, IF: 4.6, 13 citations.
[***D46***] C. Rodriguez-Emmenegger, E. Hasan, **O. Pop-Georgievski**, M. Houska, E. Brynda, A.B. Alles, Controlled/living surface-initiated ATRP of antifouling polymer brushes from gold in PBS and blood sera as a model study for polymer modifications in complex biological media, Macromolecular Bioscience 12(4) (2012) 525-532, IF: 3.7, 53 citations.
[***D47***] A.R. Kuzmyn, A. de los Santos Pereira, **O. Pop-Georgievski**, M. Bruns, E. Brynda, C. Rodriguez-Emmenegger, Exploiting end group functionalization for the design of antifouling bioactive brushes, Polymer Chemistry 5(13) (2014) 4124-4131, IF: 5.5, 54 citations.
[***D48***] N. Kasoju, N. Hawkins, **O. Pop-Georgievski**, D. Kubies, F. Vollrath, Silk fibroin gelation via non-solvent induced phase separation, Biomaterials Science 4(3) (2016) 460-473, IF: 4.2, 64 citations.
[***D49***] K.A. Milakin, D.V. Tumacder, O. Taboubi, U. Acharya, J. Hromádková, M. Lhotka, **O. Pop-Georgievski**, P. Bober, Double-Porous Polyaniline-Based Cryogels with Carbon Nanofibers for Supercapacitors, ACS Applied Energy Materials 7(8) (2024) 3354-3365, IF: 5.5, 3 citations.
[***D50***] K.A. Milakin, Z. Morávková, O. Taboubi, U. Acharya, **O. Pop-Georgievski**, P. Bober, Facile preparation of water-dispersible carboxylated polyaniline, Synthetic Metals 293 (2023) 117249, IF: 4.0, 4 citations.
[***D51***] K.A. Milakin, S. Gupta, **O. Pop-Georgievski**, Z. Morávková, U. Acharya, O. Taboubi, S. Breitenbach, N. Gavrilov, C. Unterweger, P. Bober, Macroporous nitrogen-containing carbon for electrochemical capacitors, Electrochimica Acta 418 (2022) 140370, IF: 6.6, 4 citations.
[***D52***] J. Ederer, P. Janos, P. Ecorchard, J. Tolasz, V. Stengl, H. Benes, M. Perchacz, **O. Pop-Georgievski**, Determination of amino groups on functionalized graphene oxide for polyurethane nanomaterials: XPS quantitation vs. functional speciation, RSC Advances 7(21) (2017) 12464-12473, IF: 2.9, 341 citations.

[***D53***] J. Ederer, P. Janos, P. Ecorchard, V. Stengl, Z. Belcicka, M. Stastny, **O. Pop-Georgievski**, V. Dohnal, Quantitative determination of acidic groups in functionalized graphene by direct titration, Reactive and Functional Polymers 103 (2016) 44-53, IF: 3.1, 36 citations.
[***D54***] G.S. García-Briones, R. Laga, Z. Černochová, C. Arjona-Ruiz, O. Janoušková, M. Šlouf, **O. Pop-Georgievski**, D. Kubies, Polyelectrolyte nanoparticles based on poly[N-(2-hydroxypropyl)methacrylamide-block-poly(N-(3-aminopropyl)methacrylamide] copolymers for delivery of heparin-binding proteins, European Polymer Journal 191 (2023) 111976, IF: 5.8, 9 citations.
[***D55***] H. Macková, H. Hlídková, Z. Kaberova, V. Proks, J. Kučka, V. Patsula, M. Vetrik, O. Janoušková, B. Podhorská, **O. Pop-Georgievski**, Š. Kubinová, D. Horák, Thiolated poly(2-hydroxyethyl methacrylate) hydrogels as a degradable biocompatible scaffold for tissue engineering, Materials Science and Engineering: C 131 (2021) 112500, IF: 8.5, 9 citations.
[***D56***] H. Hlidkova, I. Kotelnikov, **O. Pop-Georgievski**, V. Proks, D. Horak, Antifouling Peptide Dendrimer Surface of Monodisperse Magnetic Poly(glycidyl methacrylate) Microspheres, Macromolecules 50(4) (2017) 1302-1311, IF: 5.9, 26 citations.
[***D57***] J. Holovský, A. Peter Amalathas, L. Landová, B. Dzurňák, B. Conrad, M. Ledinský, Z. Hájková, **O. Pop-Georgievski**, J. Svoboda, T.C.-J. Yang, Q. Jeangros, Lead Halide Residue as a Source of Light-Induced Reversible Defects in Hybrid Perovskite Layers and Solar Cells, ACS Energy Letters (2019) 3011-3017, IF: 19.0, 79 citations.
[***D58***] J. Micova, M. Buryi, D. Simek, J. Drahokoupil, N. Neykova, Y.Y. Chang, Z. Remes, **O. Pop-Georgievski**, J. Svoboda, Synthesis of zinc oxide nanostructures and comparison of their crystal quality, Applied Surface Science 461 (2018) 190-195, IF: 5.2, 30 citations.
[***D59***] N. Neykova, Y.Y. Chang, M. Buryi, M. Davydova, R. Kucerkova, D. Simek, Z. Remes, **O. Pop-Georgievski**, Study of ZnO nanorods grown under UV irradiation, Applied Surface Science 472 (2019) 105-111, IF: 6.2, 37 citations.
[***D60***] N. Neykova, J. Stuchlik, K. Hruska, A. Poruba, Z. Remes, **O. Pop-Georgievski**, Study of the surface properties of ZnO nanocolumns used for thin-film solar cells, Beilstein Journal of Nanotechnology 8 (2017) 446-451, IF: 3.0, 27 citations.
[***D61***] I. Králová, D. Pilnaj, **O. Pop-Georgievski**, J. Uřičář, P. Veselý, M. Klimtová, K. Dušek, Wettability in lead-free soldering: Effect of plasma treatment in dependence on flux type, Applied Surface Science 668 (2024) 160447, IF: 6.9, 3 citations.
[***D62***] A. Schulte, A. de Los Santos Pereira, R. Pola, **O. Pop-Georgievski**, S. Jiang, I. Romanenko, M. Singh, Z. Sedlakova, H. Schonherr, R. Poreba, On-Demand Cell Sheet Release with Low Density Peptide-Functionalized Non-LCST Polymer Brushes, Macromol Biosci 23(3) (2023) e2200472 IF: 4.4, 2 citations.

References

[1] M.L. Gardel, Mol. Biol. Cell, 23 (2012) 4165-4166.
[2] B. Alberts, *et al.*, Molecular Biology of the Cell, 6th ed.2016.
[3] J.A. Davies, Extracellular Matrix, eLS, John Wiley & Sons, Ltd2001.
[4] J. Ruhe, Polymer Brushes: On the way to tailor-made surfaces, Polymer Brushes: Synthesis, Characterization, Applications Wiley-VCH Verlag GmbH & Co. KGaA 2004, pp. 1–28.
[5] B. Zhao, W.J. Brittain, Prog. Pol. Sci., 25 (2000) 677-710.
[6] W.J.B. Rigoberto C. Advincula, Kenneth C. Caster, Jurgen Ruhe, Synthesis, Characterization, Applications, WILEY-VCH Verlag GmbH & Co. KGaA,, Weinheim, 2004.
[7] W.J. Brittain, S. Minko, J. Pol. Sci. A-Pol. Chem., 45 (2007) 3505-3512.
[8] N.S. Bhairamadgi, *et al.*, Langmuir, 30 (2014) 2068-2076.
[9] J. Svoboda, *et al.*, Biomacromolecules, 20 (2019) 3453-3463.
[10] O. Pop-Georgievski, *et al.*, Langmuir, 34 (2018) 6010-6020.
[11] O. Pop-Georgievski, *et al.*, Langmuir, 28 (2012) 14273-14283.
[12] O. Pop-Georgievski, *et al.*, Biomacromolecules, 12 (2011) 3232-3242.
[13] R. Sivkova, *et al.*, Int. J. Mol. Sci., 21 (2020) 6800.
[14] V. Proks, *et al.*, New Biotech., 29 (2012) S154-S154.
[15] A. de los Santos Pereira, *et al.*, Biomacromolecules, 17 (2016) 1179-1185.
[16] N.Y. Kostina, *et al.*, Macromol. Biosci., 16 (2016) 83-94.

[17] O. Pop-Georgievski, C. *et al.*, J. Mat. Chem. B, 1 (2013) 2859-2867.
[18] V. Proks, *et al.*, Macromol. Biosci., 12 (2012) 1232-1242.
[19] R. Poreba, *et al.*, Macromol. Biosci., 20 (2020) e1900354.
[20] H. Lisalova, *et al.*, Anal. Chem., 89 (2017) 3524-3531.
[21] T. Riedel, *et al.*, Anal. Chem., 89 (2017) 2972-2977.
[22] H. Vaisocherova-Lisalova, *et al.*, Anal. Chem., 88 (2016) 10533-10539.
[23] T. Riedel, *et al.*, Biosens. Bioel., 85 (2016) 272-279.
[24] C. Selhuber-Unkel, *et al.*, Biophys. J., 98 543-551.
[25] L.J. Vega, *et al.*, Biomacromolecules, 15 (2014) 2172-2179.
[26] S.H. Kristensen, G.A. Pedersen, L.N. Nejsum, D.S. Sutherland, Nano Lett., 12 (2012) 2129-2133.
[27] T. Wolfram, *et al.*, BMC Cell Biol, 9 (2008) 64.
[28] J. Blummel, *et al.*, Biomaterials, 28 (2007) 4739-4747.
[29] S. Rahmouni, *et al.*, Adv. Mater., 25 (2013) 5869-5874.
[30] F. Rechenmacher, *et al.*, Angew. Chem. Int. Ed., 52 (2013) 1572-1575.
[31] E.A. Cavalcanti-Adam, *et al.*, Biophys. J., 92 (2007) 2964-2974.
[32] M. Arnold, *et al.*, Nano Lett., 8 (2008) 2063-2069.
[33] A.G. de Beer, *et al.*, Phys. Rev. E Stat. Nonlin. Soft Matter Phys., 81 (2010) 051914.
[34] J.P. Spatz, *et al.*, Langmuir, 16 (2000) 407-415.
[35] M. Arnold, *et al.*, Soft Matter, 5 (2009) 72-77.
[36] L. Maus, *et al.*, Langmuir, 25 (2009) 7910-7917.
[37] Y. Cao, *et al.*, Plast. Rec. Surg., 100 (1997) 297-304.
[38] T.Y. Lu, *et al.*, Nat. Commun., 4 (2013) 2307.
[39] S.E. Motta, *et al.*, NPJ Reg. Med., 4 (2019) 14.
[40] K. Schenke-Layland, *et al.*, Cardiovasc. Res., 60 (2003) 497-509.
[41] B. Maher, Nature, 499 (2013) 20-22.
[42] W. Xue, *et al.*, ACS App. Bio. Mat., 2 (2019) 3820-3827.
[43] A. Foerster, M. Duda, H. Kraśkiewicz, M. Wawrzyńska, H. Podbielska, M. Kopaczyńska, Physico-chemical stent surface modifications, Functionalised Cardiovascular Stents, Woodhead Publishing 2018, pp. 137-148.
[44] J.M. Seeger, *et al.*, J. Vasc. Surg., 22 (1995) 327-336.
[45] F. Surman, *et al.*, Macromol. Biosci., 15 (2015) 636-646.
[46] H. Zhang, M. Chiao, J. Med. Biol. Eng., 35 (2015) 143-155.
[47] A.L. Lewis, *et al.*, Biomaterials, 21 (2000) 1847-1859.
[48] S. Sharma, *et al.*, Langmuir, 20 (2004) 348-356.
[49] H. Shin, *et al.*, Biomaterials, 24 (2003) 4353-4364.
[50] M.F. Brizzi, *et al.*, Curr. Op. Cell Bio., 24 (2012) 645-651.
[51] J.A. McDonald, Ann. Rev. Cell Bio., 4 (1988) 183-207.
[52] A. Halperin, M. Kröger, Langmuir, 28 (2012) 16623.
[53] Y. Yu, *et al.*, Nanoscale, 9 (2017) 1670-1675.
[54] Y. Zhang, *et al.*, J. Phys. Chem. C, 111 (2007) 8916-8924.
[55] Y. Zhang, *et al.*, J. Am. Chem. Soc., 127 (2005) 14505-14510.
[56] J. Lahann, John Wiley & Sons Ltd, 2009.
[57] S. Perrier, Macromolecules, 50 (2017) 7433-7447.
[58] A.M. Elsen, *et al.*, Macromolecules, 44 (2011) 1752-1754.
[59] H. Willcock, R.K. O'Reilly, Pol. Chem., 1 (2010) 149-157.
[60] K. Matyjaszewski, *et al.*, Langmuir, 23 (2007) 4528-4531.
[61] T. Zhang, *et al.*, Polym. Chem., 5 (2014) 4790-4796.
[62] S. Edmondson, *et al.*, Chem. Soc. Rev., 33 (2004) 14-22.
[63] D.M. Jones, W.T.S. Huck, Adv. Mat., 13 (2001) 1256-1259.
[64] U. Mansfeld, *et al.*, Pol. Chem., 1 (2010) 1560-1598.
[65] D. Jirak, *et al.*, Chem. Commun., 57 (2021) 4718-4721.
[66] M. Vorobii, *et al.*, Biomacromolecules, 20 (2019) 959-968.
[67] M. Vorobii, *et al.*, Pol. Chem., 7 (2016) 6934-6945.
[68] M.J. Rust, *et al.*, Nat. Methods, 3 (2006) 793-795.

[69] S.T. Hess, *et al.*, Biophys. J., 91 (2006) 4258-4272.
[70] E. Betzig, *et al.*, Science, 313 (2006) 1642-1645.
[71] B. Knoll, F. Keilmann, Nature, 399 (1999) 134-137.
[72] F. Keilmann, R. Hillenbrand, Philos. Trans. R. Soc. A-Math. Phys. Eng. Sci., 362 (2004) 787-805.
[73] R. Hillenbrand, *et al.*, Nature, 418 (2002) 159-162.
[74] F. Huth, *et al.*, Nano Lett., 13 (2013) 1065-1072.
[75] A.A. Govyadinov, *et al.*, J. Phys. Chem. Lett., 4 (2013) 1526-1531.
[76] I. Amenabar, *et al.*, Nat. Commun., 4 (2013) 9.
[77] S. Mastel, *et al.*, Appl. Phys. Lett., 106 (2015) 5.
[78] I. Amenabar, *et al.*, Nat. Commun., 8 (2017) 10.
[79] M. Brehm, *et al.*, Nano Lett., 6 (2006) 1307-1310.
[80] C. Westermeier, *et al.*, Nat. Commun., 5 (2014) 4101.
[81] F. Huth, *et al.*, Nano Lett., 12 (2012) 3973-3978.
[82] A. Dazzi, C.B. Prater, Chem. Rev., 117 (2017) 5146-5173.
[83] M. Ryu, *et al.*, Appl. Sci., 9 (2019) 3991.
[84] A. Cernescu, *et al.*, Anal. Chem., 90 (2018) 10179-10186.
[85] L. Mester, *et al.*, Nat. Commun., 11 (2020) 3359.
[86] A. de los Santos Pereira, *et al.*, Anal. Chem., 92 (2020) 4716-4720.
[87] K.J. Kaltenecker, *et al.*, Sci. Rep., 11 (2021) 21860.
[88] D.F. Dorado Daza, *et al.*, Polymer, 323 (2025) 128175.
[89] Y.M. Wang, *et al.*, Pol. Chem., 13 (2022) 3815-3826.
[90] Y.M. Wang, *et al.*, Pol. Chem., 15 (2024) 2070-2080.
[91] A. Schulte, *et al.*, Macromol. Biosci., 23 (2023) e2200472.
[92] O. Pop-Georgievski, *et al.,* Beilstein J. Nanotechn., 6 (2015) 617-631.
[93] O. Pop-Georgievski, *et al.*, Thin Solid Films, 543 (2013) 180-186.
[94] V. Proks, *et al.*, Macromol. Chem. Phys., 214 (2013) 499-507.
[95] N.F. Della Vecchia, *et al.*, Adv. Funct. Mater., 23 (2013) 1331-1340.
[96] S. Hong, *et al.*, Adv. Funct. Mater., 22 (2012) 4711-4717.
[97] B. Bilinska, Spectr. Acta A-Mol.Biomol. Spec., 52 (1996) 1157-1162.
[98] F. Yu, *et al.*, J. Mol. Struct, 982 (2010) 152-161.
[99] M. Kral, *et al.*, Colloids. Surf. B Biointerfaces, 235 (2024) 113769.
[100] M. Kral, *et al.*, Colloids Surf. B Biointerfaces, 221 (2023) 112954.
[101] J. Svoboda, *et al.*, Colloids Surf. B: Biointerfaces, 205 (2021) 111897.
[102] J. Musilkova, *et al.*, J. Mater. Sci.: Mater. Med., 26 (2015) 253.
[103] J. Svoboda, *et al.*, Macromol. Rap. Comm., 44 (2023) e2300168.
[104] T.A. Tunca Arın, *et al.*, Mat. Today Bio, 31 (2025) 101462
[105] O. Kopilec, *et al.*, Macromol. Chem. Phys., 226 (2025) 70001.
[106] S. Slavin, *et al.*, Soft Matter, 8 (2012) 118-128.
[107] E. Mazl Chanova, *et al.*, Biomater. Sci., 5 (2017) 1130-1143.
[108] R. Zimmermann, *et al.*, Soft Matter, 10 (2014) 7804-7809.
[109] R. Zimmermann, *et al.*, Curr. Opp. Coll. Interface Sci., 18 (2013) 83-92.
[110] R. Zimmermann, *et al.*, Langmuir, 21 (2005) 5108-5114.
[111] B. Leibauer, *et al.*, Adv. Funct. Mater., 35 (2025) 2419443.
[112] B. Leibauer, *et al.*, J. Am. Chem. Soc., 146 (2024) 10073-10083.
[113] R. Sivkova, *et al.*, Prog. Org. Coat., 178 (2023) 107447.
[114] C. Rodriguez-Emmenegger, *et al.*, Adv. Mat., 25 (2013) 6123-6127.
[115] D. Abt, *et al.*, Chem.-Eur. J., 21 (2015) 13186-13190.
[116] M. Singh, *et al.*, Pol. Chem., 15 (2024) 3300-3310.
[117] N.Y. Kostina, *et al.*, Macromol. Biosci., 19 (2019) e1800403.
[118] J. Laun, *et al.*, Macromol. Rapid Commun., 36 (2015) 1681-1686.
[119] M. Vorobii, *et al.*, Pol. Chem., 6 (2015) 4210-4220.
[120] C. Rodriguez-Emmenegger, *et al.*, Macromol. Rapid Comm., 32 (2011) 952-957.
[121] Z. Riedelova, *et al.*, Macromol. Biosci., 22 (2022) e2200247.
[122] T. Riedel, *et al.*, Macromol. Biosci., (2022) 2100460.

[123] C. Dalvit, *et al.*, Chem-Eur J, 20 (2014) 11058-11068.
[124] S. Lee, *et al.*, Langmuir, 24 (2008) 4817-4826.
[125] C. Zhao, *et al.*, Biomaterials, 34 (2013) 4714-4724.
[126] M. Vorobii, *et al.*, Pol. Chem., 6 (2015) 4210-4220.
[127] C. Rodriguez-Emmenegger, *et al.*, Macromol. Biosci., 12 (2012) 1413-1422.
[128] A.R. Kuzmyn, *et al.*, Polym. Chem., 5 (2014) 4124-4131.
[129] C. Zhao, *et al.*, Langmuir, 27 (2011) 4906-4913.
[130] N. Kasoju, *et al.*, Biomater. Sci., 4 (2016) 460-473.
[131] K.A. Milakin, *et al.*, ACS Appl. Energy Mat., 7 (2024) 3354-3365.
[132] K.A. Milakin, *et al.*, Electrochim. Acta, 418 (2022) 140370.
[133] J. Ederer, *et al.*, RSC Adv., 7 (2017) 12464-12473.
[134] J. Ederer, *et al.*, React. Funct. Polym., 103 (2016) 44-53.
[135] G.S. García-Briones, *et al.*, Eur. Polym. J., 191 (2023) 111976.
[136] H. Macková, *et al.*, Mat. Sci. Eng. C, 131 (2021) 112500.
[137] H. Hlidkova, *et al.*, Macromolecules, 50 (2017) 1302-1311.
[138] J. Holovský, *et al.*, ACS Energy Lett., (2019) 3011-3017.
[139] M. Buryi, *et al.*, Optical Materials, 145 (2023) 114445.
[140] J. Micova, *et al.*, Appl. Surf. Sci., 461 (2018) 190-195.
[141] N. Neykova, , Appl. Surf. Sci., 472 (2019) 105-111.
[142] N. Neykova, *et al.*, Beilstein J. Nanotechnol., 8 (2017) 446-451.
[143] I. Králová, *et al.*, Appl. Surf. Sci., 668 (2024) 160447.
[144] I. Romanenko, *et al.*, Polymer, 332 (2025) 128569.
[145] R.R. Patil, *et al.*, ACS Macro Lett., 4 (2015) 251-254.
[146] C. Kang, *et al.*, Pol. Chem., 7 (2016) 302-309.
[147] C.J. Kang, *et al.*, Macromolecules, 47 (2014) 269-275.
[148] C.B. Anfinsen, J.T. Edsall, F.M. Richards, Advances in Protein Chemistry, Academic Press1986, pp. 181-364.
[149] A. Barth, C. Zscherp, Quart. Rev. Biophy., 35 (2003) 369-430.
[150] F.S. Ruggeri, *et al.*, Nat. Comm., 6 (2015) 7831.
[151] F.S. Ruggeri, *et al.*, Sci. Rep., 6 (2016) 31155.
[152] A. Dazzi, *et al.*, Appl. Spec., 66 (2012) 1365-1384.

Statement about the authorship of the presented research results:

In the majority of the presented research results the contribution of the author, Ognen Pop-Georgievski, of this Thesis was pivotal, designing concepts of the described systems, performing syntheses and experimental measurements, data processing and interpretation, suggesting and developing novel experimental and surface characterization methodologies, formulating hypothesis and deriving conclusions on basis of obtained results, as well as supervising of bachelor degree and Ph.D. students during their research work (Ondřej Kopilec, Kristina Dušková, Yu-Min Wang, Iryna Romanenko and Diego Fernando Dorado Daza).

I acknowledge the precious contributions of colleagues from my group and institute (Dr. Andres de los Santos Pereira, Dr. Vladímir Proks, Dr. Tomas Riedel, Dr. Cesar Rodriguez-Emmenegger, Dr. Jan Svoboda, Dr. Radoslava Sivkova, Dr. Patrycja Bober, Dr. Rafal Poreba, Dr. Dana Kubies), as well as from our national (Dr. Neda Neykova, Ass. Prof. Jakub Holovský, Prof. Pavel Janos, Prof. Jiři Homola, Prof. Pavel Matějka, Ass. Prof. Ondřej Sedláček) and from international (Dr. Adrian Cernescu, Dr. Fritz Keilman, Dr. Anna Kalozsi, Prof. Carsten Werner, Prof. Patrick Koelsch, Prof. Christopher Barner-Kowollik, Prof. Virgil Percek, Prof. Hans-Jürgen Butt) collaboration networks.

I sincerely thank all my students and colleagues who collaborated with me on the presented research. Presented research and Thesis would not have been possible without their valuable contributions.

I acknowledge the use of AI-based language editing tools for improving the clarity and style of the English text in this Thesis.